STUDY ON EPOXY BASED COMPOSITES FOR HIGH TEMPERATURE MOLDING COMPOUNDS

A Dissertation
Presented to
The Academic Faculty

by

Fan Wu

In Partial Fulfillment
of the Requirements for the Degree
Master's Degree in the
Materials Science and Engineering

Georgia Institute of Technology
August 2018

STUDY ON EPOXY BASED COMPOSITES FOR HIGH TEMPERATURE MOLDING COMPOUNDS

Approved by:

Dr. CP Wong, Advisor
School of Materials Science and Engineering
Georgia Institute of Technology

Dr. Meilin Liu
School of Materials Science and Engineering
Georgia Institute of Technology

Dr. Z. John Zhang
School of Chemical and Biomolecular Engineering
Georgia Institute of Technology

Date Approved: [July 18, 2018]

[To my family for their love and support, and to my friends for being part of my journey]

ACKNOWLEDGEMENTS

First of all, I would like to express my deepest thanks to my advisor, Prof. C. P. Wong, for his support, guidance and inspiration, without which I wouldn't be able to complete my study in Georgia Tech. I also want to acknowledge my committee members Prof. Meilin Liu and Prof. Z. John Zhang for their valuable comments and constructive suggestions to my work.

I want to thank all the help and advice I received from the members in Prof. Wong's group and other fellow colleagues: Dr. Kyoung-Sik Moon, Dr. Chia-Chi Tuan, Dr. Bo Song, Dr. Yun Chen, Dr. Weimin Yang, Mr. Cheng Zhang, Dr. Gang Jian, Dr. Lixi Wang, Mr. Jinho Hah, Mr. Jiaxiong Li, Dr. Xiaona Wang, Dr. Rongli Zhang, Ms. Lin Chen, Ms. Yi Lu, Ms. Yi Li, Ms. Yulian Yao and Ms. Annie Wang. I want to thank the undergraduate student, Mr. Mitchell Nicolas, who worked with me for one semester.

I would like to appreciate Georgia Tech 3D Packaging Research Center for partially supporting my work. I also want to give my special thanks to the members from Georgia Tech 3D Packaging Research Center for sharing their insights on my research: Prof. Rao Tummala, Dr. Pulugurtha Raj, Dr. Vanessa Smet, Mr. Christopher White, Mr. Haksun Lee, Ms. Shreya Dwarakanath.

Lastly, I am indebted to my parents, Yunsheng Wu and Qi Chen, for their endless love and support during my study abroad in the United States.

TABLE OF CONTENTS

LIST OF TABLES

LIST OF FIGURES

LIST OF SYMBOLS AND ABBREVIATIONS

AFM	atomic force microscopy
Al_2O_3	aluminum oxide
BJT	bipolar junction transistor
BN	boron nitride
C_p	heat capacity
CNT	carbon nanotube
CTE	thermal expansion coefficient
DICY	dicyandiamide
DSC	differential scanning calorimetry
DMA	dynamic mechanical analysis
EMC	epoxy molding compounds
FTIR	fourier transform infrared spectra
GaN	gallium nitride
K_{IC}	critical stress intensity factor
IC	integrated circuit
JFET	junction field effect transistor
M_t	water absorption
POSS	polyhedral oligomeric silsesquioxane
SEM	scanning electron microscopy
Si	silicon
SiC	silicon carbide
SiO_2	silicon dioxide

T_g	glass transition temperature
T_J	maximum junction temperature
TGA	thermogravimetric analysis
TMA	thermomechanical analysis
W_0	Sample dry weight
W_t	sample wet weight
WBG	wide bandgap
XRD	X-ray diffraction
α	thermal conductivity
κ	thermal conductivity
ΔH	enthalpy change
θ_{J_A}	total thermal resistance of the cooling system
P	density

SUMMARY

Epoxy molding compound (EMC) is one of the most widely used encapsulation materials for electronic packaging. To provide substantial protection for the electronic packages, EMCs are frequently required to work at elevated temperature, especially when high power and high density devices are developing rapidly and more heat is generated during operation.

This thesis discussed the study on epoxy based composites for high temperature molding compounds by investigating two components most important in EMC system, namely the polymer resin (Chapter 2 and 3) and the filler system (Chapter 4).

In order to increase the glass transition temperature (T_g) and thermal stability of epoxy resin, cyanate ester was incorporated into the polymer matrix. The copolymer network formed by epoxy and cyanate ester (CE/EP) exhibited excellent thermal stability and high T_g above 270 ℃ because of the thermally stable *s*-triazine structures formed by cyanate ester trimerization. However, cyanate ester was affected by the hydrolysis reaction and too much cyanate ester in the system led to blistering and T_g drops in high temperature and high humidity tests. The cyanate ester amount in this copolymer was optimized to be 33-50 %. Polyimide was incorporated into CE/EP system as an additive (CE/EP-PI) to further improve the thermal stability of this epoxy-based resin. Aromatic polyimide exhibited good compatibility with CE/EP for their structural similarity. Improvements in T_g, storage modulus, fracture toughness and long term high temperature performance were observed at 5-10 % polyimide loading. At high polyimide loading

level (> 10 %), a secondary phase emerged which deteriorated the resin properties such as storage modulus.

The second part of this thesis investigated a modified filler system with surface coated silicon carbide (SiC) for thermal conductivity enhancement. Accounting for 70-90 % of EMC, fillers determine the properties of the EMCs to a large extent. At high filler loading level, more contacts between fillers are created, which potentially provides more thermally conductive paths for heat transfer. In this part, SiC with high thermal conductivity was adopted as a replacement for conventional silica fillers. After surface treatment by silane coupling agent (SiC-GPTMS) and reactive silicon rubber (SiC-A15), modified SiC increased the thermal conductivity of the composites from 0.11 W/mK to 0.28 W/mK at 30 % filler loading. While composites with these two types of modified SiC showed similar performance in thermal conductivity and fracture toughness, they had different morphology when incorporated into the polymer matrix. SiC-GPTMS had a better dispersity in epoxy, but SiC-A15 aggregated and formed separated filler regions due to the strong interaction between the reactive rubber layers. However, the reactive rubber layers also provided better filler-matrix interface and prevented the crack propagation along the interface.

In this thesis, the research on epoxy resin provided a valuable insight into the structural-property relation in epoxy-based copolymer and polymer blends, which can guide the development of polymer matrix for high temperature EMCs. The work on SiC fillers shed more light on effect of high thermally conductive fillers and surface treatments on epoxy composites.

CHAPTER 1. INTRODUCTION

1.1 Epoxy Molding Compounds

1.1.1 Introduction of Epoxy Molding Compounds

Electronic encapsulation materials are quite important in an electronic package for protecting the integrated circuits (ICs) and other electronic components from external forces, such as heat, moisture, pressure and chemical corrosion. Compared with other conventional encapsulation materials such as metals and ceramics, polymer materials have the advantage of low cost and eligibility for mass production.[1] With the development of polymer technology, the reliability of polymer encapsulation materials is no longer a major concern. Materials such as epoxy,[2-3] silicone,[4-5] polyimide[6-7] and polysulfide[8-9] have been applied as encapsulants for electronic devices. Among all different kinds of polymer-based encapsulation materials, epoxy molding compounds (EMCs) are one of the most widely used materials in electronic packaging industry for its outstanding performance in adhesion, chemical resistance and modulus.[10] Different forms of EMCs including pellet and granular are shown in Figure 1.1. Generally, EMCs consist of 10-20 % of epoxy and hardener, which builds up the crosslinking polymer network and gives excellent adhesion strength. A heavy loading of filler, usually more than 70 %, is added into the EMCs to lower the thermal expansion coefficient (CTE), provide higher modulus and lower the moisture absorption of the compounds. Besides, varieties of different additives are included in the finalized products. For example, silane coupling agents are intensively used to improve the interface between the polymer matrix and the filler, which enables a better compatibility of the silica filler in the compounds. Catalysts

are used to promote the curing reaction of epoxy and hardener, and flame retardants are used to reduce the overall flammability of the compounds. Figure 1.2 shows the components of a typical EMC.

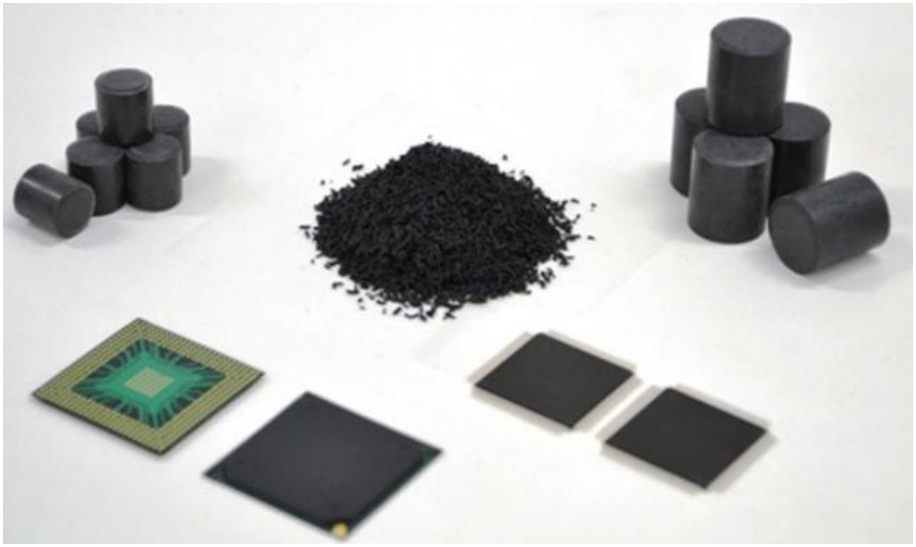

Figure 1.1– Different forms of EMCs[10]

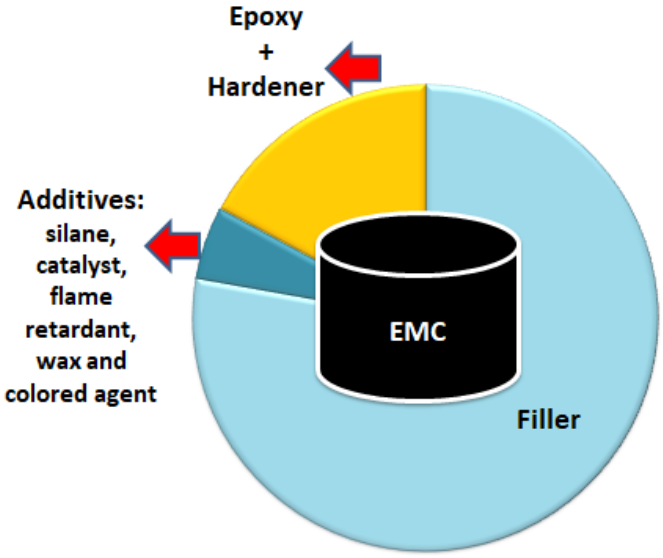

Figure 1.2 – Components of a typical EMC

1.1.2 Molding Methods for EMCs

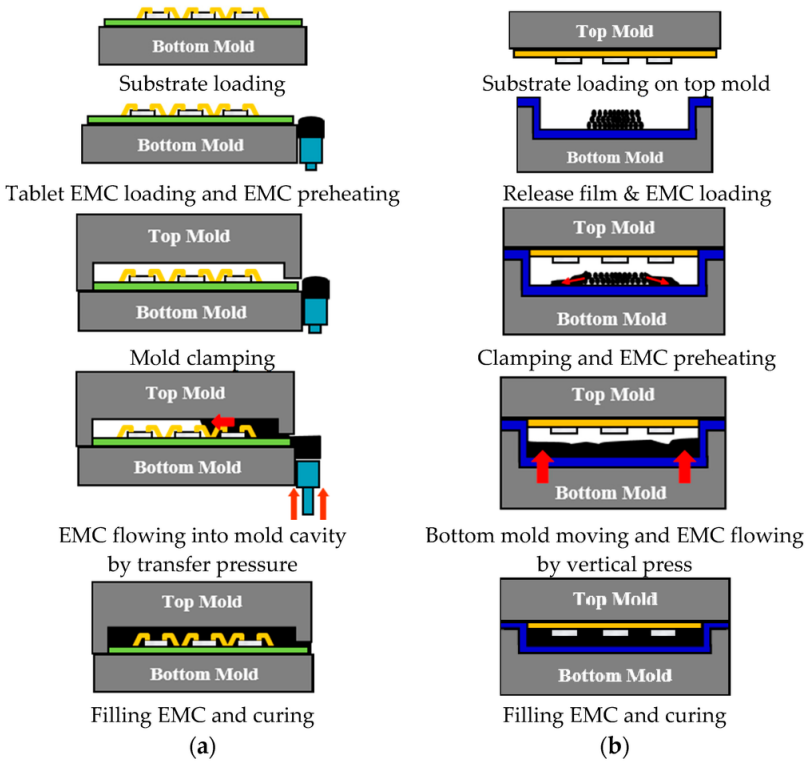

Figure 1.3 – Process of (a) transfer molding method (b) compression molding method[11]

In the packaging process of EMCs, transfer molding and compression molding are two molding methods mainly adopted in industry nowadays. Figure 1.3 shows the process of transfer molding and compression molding, respectively.[11] These two methods have different characteristics. For transfer molding, EMC is pre-heated in the charge and pushed into the mold cavity under pressure. After heating and curing, the molded product is released from the cavity. This short production cycle of transfer molding makes it suitable for mass production. However, the runner and cull parts attached to the molded products after transfer molding need to be removed, which causes more waste of the materials compared to compression molding. For compression molding, usually granular or power form of EMC is weighted and put into the mold. The upper part of the mold

than press the raw materials to fit in the mold cavity with a specific design of shape. Wasting fewer materials than transfer molding, compression molding also has a shorter flow distance, which reduces the chance of filler segregation during molding.

1.1.3 Epoxy Resin

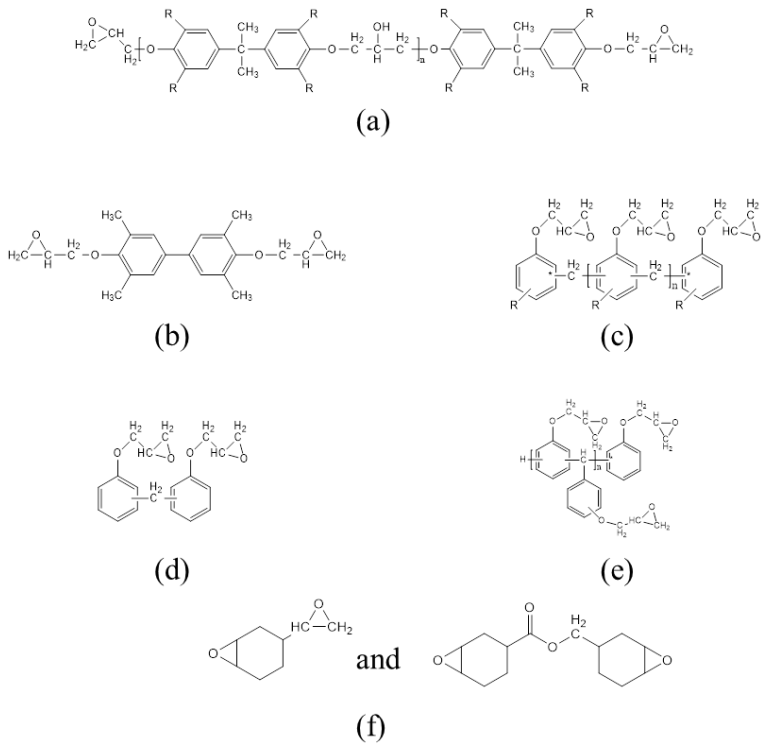

Figure 1.4 – Chemical structures of (a) bisphenol A epoxy (b) biphenyl epoxy (c) novolac epoxy (d) bisphenol F epoxy (e) multifunctional epoxy (f) cycloaliphatic epoxy

Epoxy is a type of chemical with an epoxide ring which can open and react with various of chemicals including amine, anhydride, phenols, and so forth. This ring opening reaction is the basis of the construction of polymer crosslinking network in the EMCs, where epoxy is cured by hardeners such as dicyandiamide (DICY), novolac phenolic resins, anhydrides and amines.[12] The hardener usually has a functionality larger than two, which enables it to build the crosslinking network with epoxy. Scheme 1.1 shows a

typical reaction between epoxy and diamine. In this reaction, each diamine molecule can react with four epoxide groups. The hydroxyl groups formed after ring opening in EMC provide good adhesion strength of epoxy, which is one of the most desirable properties of epoxy resin for its application in electronic packaging. A variety of epoxy resins can be applied in the molding compounds. Figure 1.4 shows the structures of several different epoxy resins, including bisphenol A epoxy, bisphenol F epoxy, biphenyl epoxy, novolac epoxy, multifunctional epoxy and cycloaliphatic epoxy. The difference in structures of the epoxies provides them with different characteristics. For example, biphenyl epoxy has low viscosity and multifunctional epoxy provides higher crosslinking density.

Scheme 1.1 – Reaction between epoxy and diamine

1.1.4 Development of EMCs

Recently, in the development of EMCs, novel structures and additives have been proposed and investigated to achieve better performance in flammability, toughness and thermal conductivity. Wang *et al*, reported a grafted polyphosphamide functionalized graphene as flame retardant for epoxy composites, which provided superior fire resistance.[13] Domun *et al* reported the improvement of fracture toughness in epoxy compounds by nanomaterials such as carbon nanotubes (CNTs), graphene, nanoclay and nanosilica.[14] Gu *et al* developed a boron nitride filled (60%) epoxy composite with a thermal conductivity high than 1 W/mK.[15] However, with the ever-evolving electronic

industry, more and more requirements are imposed on EMC, such as high temperature resistance. Furthermore, properties including viscosity, dielectric constant, loss factor, CTE and adhesion strength also need to be taken into consideration in the evaluation and development of EMC, which determines the potential application and commercialization of EMC in electronic industry.

1.2 Challenges and Research Objectives

1.2.1 Challenges of Epoxy Molding Compounds

Wide bandgap (WBG) semiconductors such as silicon nitride (SiC) and gallium nitride (GaN) have advantages over silicon (Si) in various aspects including larger energy gap, higher electric breakdown field, higher saturated electron velocity and better electron mobility.[16] Therefore, WBG semiconductors have the ability to facilitate the high frequency operation, which is essential in the miniaturization of power devices.[17] One of the major challenges facing the development of WBG semiconductors is thermal management issue. Most of the failures in semiconductor equipment are due to the excessive operation temperature, which becomes increasing concerning, especially for WBG semiconductors with high junction temperature.[17] The maximum junction temperature (T_J) of SiC can reach above 200 ℃. The T_J of 4H-SiC JFETs and BJTs exceeds 250 ℃ easily even with a low ambient temperature, as reported by Sheng (Figure 1.5).[18] This increasing trend in temperature is challenging the reliability of encapsulation materials such as EMCs which have trouble working continuously above 180 ℃.[19]

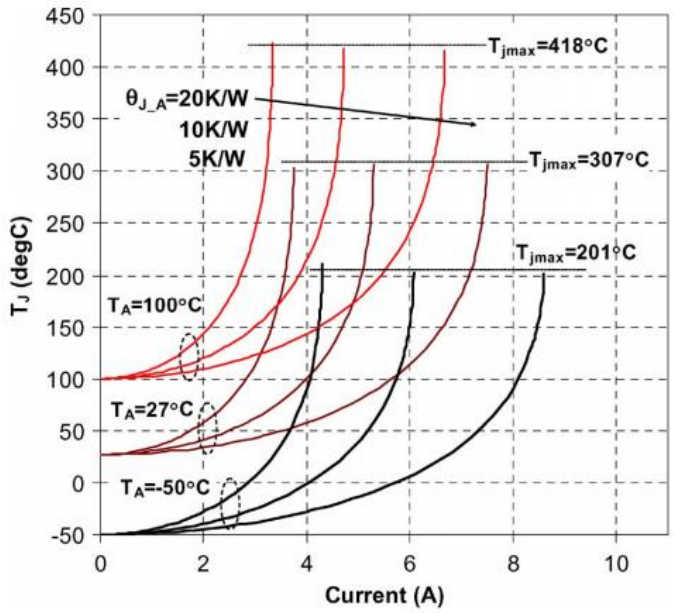

Figure 1.5 – Junction temperature of 4H-SiC JFETs and BJTs[18]

EMCs experience deterioration in properties when exposed under high temperature for a long period of time, which is referred as material aging. Increased modulus, embrittlement and decreased fracture toughness are observed after aging, which promotes the crack propagation in EMC and results in material failures.[20] A variety of aging reactions are involved in the EMC system subjected to high temperature, among which thermo-oxidation reaction is one of the most important. The oxidation layer of EMC can be observed by fluorescence microscopy as shown in Figure 1.6.[21] Oxygen diffused into the molding compounds reacts with the polymer network, generates radicals and alters the network structure. On one hand, radicals formed in thermo-oxidation continue to react with the other part polymer, resulting in regions with high crosslinking density. One the other hand, they break down the polymer backbone as well. Regions with different crosslinking densities and T_g are formed after long term high temperature

aging.[21] Detailed mechanism and influence of thermo-oxidation reaction in epoxy resin is discussed in 2.3.5.

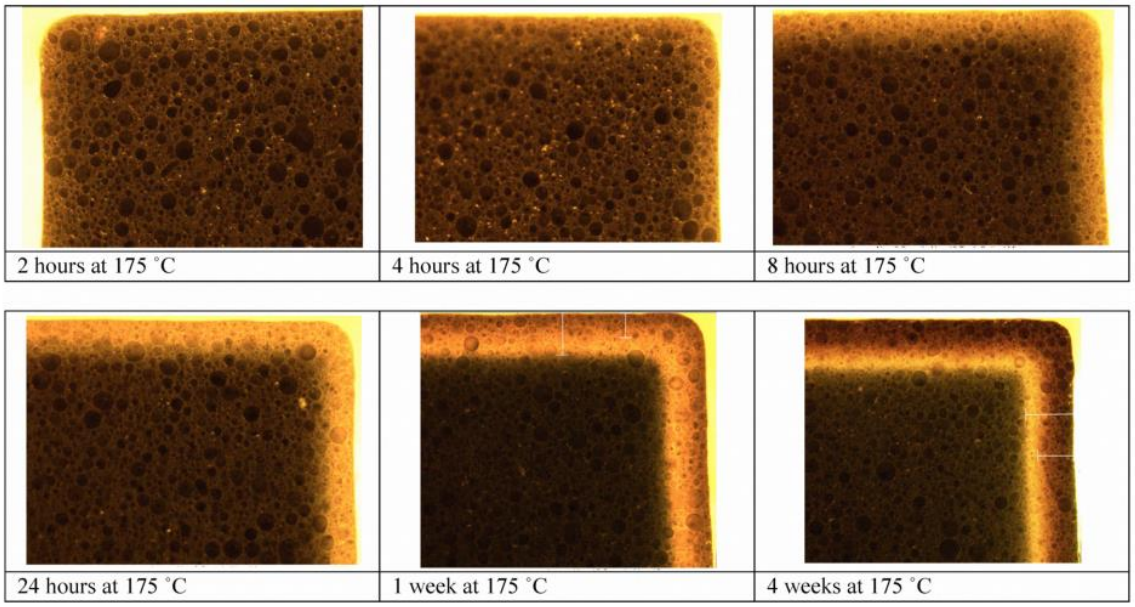

Figure 1.6 – Fluorescence microscope images of EMC under thermos-oxidation[21]

1.2.2 Thermal Conductivity of Epoxy Resin

With the development of WBG semiconductors, more heat is generated in the package, which imposes more stringent requirements on the heat management. Therefore, the thermal conductivity of EMC becomes increasingly important. Atomic vibrational waves, which is also refer as phonons, are responsible for the thermal conduction in epoxy resin. When a phonon goes across an interface, it changes from one energy state to another which causes a thermal interfacial resistance. This resistance depends not only on the defects of the surface, but also on the available energy states on both sides of the interface. For most of the polymers, phonons scatter when they transfer from one chain to another, resulting in a low thermal conductivity. It is possible for some of the

thermoplastic polymers to exhibit a high thermal conductivity due to their unique chain structure such as π–conjugated polymers (Figure 1.7).[22] However, for epoxy, as a thermoset polymer, it usually has thermal conductivity as low as 0.2-0.3 W/mK.[23] Although highly oriented polymer matrix provides a high thermal conductivity, it is not cost-effective as an encapsulation material for mass production in electronic packaging.

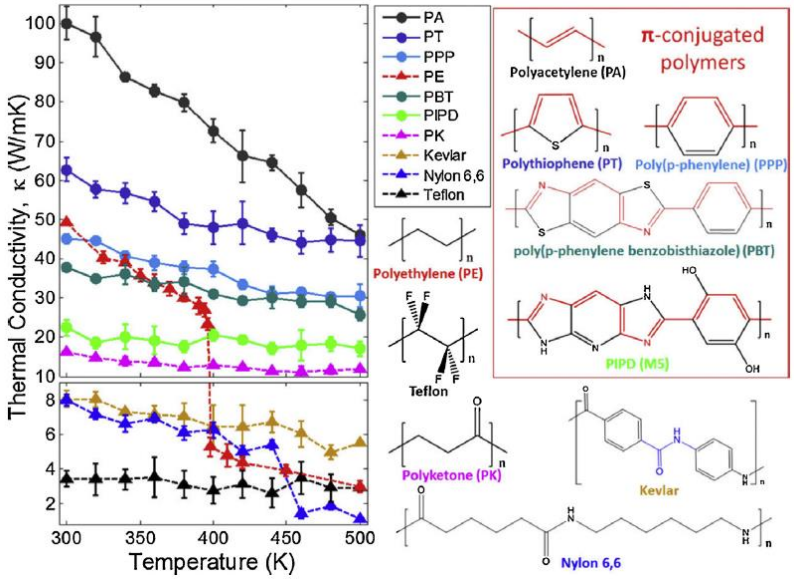

Figure 1.7 – Thermal conductivity and structure of polymer[22]

Therefore, more focus has been put on the filler modification for high thermal conductivity. Metal filler has high thermal conductivity. Zhou *et al* fabricated silica coated self-passivated aluminium fibers and nanoparticles as filler for polymer composites, which reached a highest thermal conductivity of 15.2 W/mK at 50 vol.% filler loading (Figure 1.8).[24] Providing high thermal conductivity, metal based filler also results in high loss factor and high permittivity which is not desirable for high power device packaging. Electrically non–conductive ceramic fillers such as boron nitride (BN) and silicon carbide (SiC) have high thermal conductivity as well as excellent dielectric

properties, which make them promising candidate for EMC. Huang *et al* reported a polyhedral oligosilsesquioxane-modified boron nitride nanotube (BNNT) filler for epoxy composites with a thermal conductivity of ~3 W/mK at a 30% filler loading (Figure 1.9). Although high thermal conductivity can be achieved by applying high thermal conductivity ceramic filler with high aspect ratio such as BNNT, viscosity is another issue that restricts this application. Filler with high aspect ratio gives more contacts between fillers, which is advantageous for phonon transfer and enables a high thermal conductivity. However, more contacts between fillers also lead to more friction and a higher viscosity, especially for EMC containing a large amount of filler.

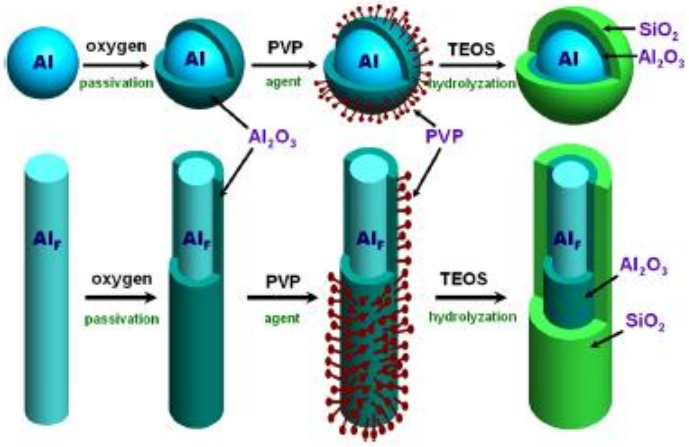

Figure 1.8 – Structure of silica coated self-passivated aluminum fibers[24]

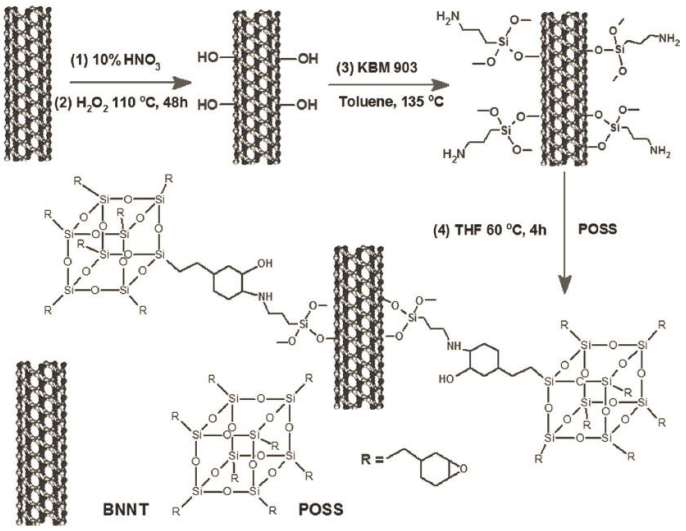

Figure 1.9 – Structure of polyhedral oligosilsesquioxane-modified BNNTs

1.2.3 Research Objectives

As described above, it is necessary to develop epoxy molding compounds that can work under high temperature for application in harsh environment such as fields of aerospace and automotive, and for application in the next generation of high power devices where more heat is generated.

1.2.3.1 High Glass Transition Temperature (T_g)

T_g is a secondary phase transition temperature at which polymers transfer from glass state to rubber state with increased chain mobility. It can be used to determine the application temperature of a polymer. In this work, we are aiming at a T_g high than 250 ℃, which is a prerequisite for a high temperature epoxy resin.

1.2.3.2 High Thermal Conductivity

Considering the high filler loading amount in EMC, improvement in the thermal conductivity of filler system can be a big help in promoting the overall thermal conductivity of EMC. Conventional silica filler has a thermal conductivity around 1.3 W/mK, while some other ceramic materials, such as silicon carbide (SiC), have much high thermal conductivity. By incorporating SiC as part of the filler system, a high thermal conductivity of the EMC can be achieved.

CHAPTER 2. CYANATE ESTER/EPOXY COPOLYMER SYSTEM

Epoxy molding compounds (EMCs) have become an integral component for high power electronics to work under harsh environment nowadays. For high temperature operation, polymer networks with high glass transition temperature (T_g) are required to ensure device stability. In this chapter, high T_g polymers were designed via controlled incorporation of *in-situ* formed and thermally stable triazine structures into epoxy matrix.

2.1 Background

The electronic industry has witnessed rapid development recently due to the increasing demands for high power electronics, such as high frequency power converters, motor controls, power supplies, etc.[25-27] As the continuous scaling of these high-end devices, heat generation and accumulation can become a critical issue. To overcome thermal issues and ensure system operation, new material designs are required to construct electronic packages with improved high temperature reliability. Epoxy molding compounds (EMCs), as a type of encapsulation materials, have been widely used in microelectronics because of their outstanding and balanced performance in adhesion strength, elastic modulus, chemical resistance, and moisture resistance.[28-29] However, thermo-oxidative degradation is typically observed in epoxy resins, which leads to enlarged modulus, reduced strains, and mass loss during thermal aging. Thermal aging of epoxy resins have been reported to involve the formation of various carbonyl groups and occurrence of bond breaking in C-C and C-O.[30-33] It is possible to form ketone and ester

groups through oxidation of methylene groups and tertiary hydrogen, with chain scission and chain rearrangement. To address the thermal instability problem, recent studies have tried to incorporate organic or inorganic additives to tune the thermal and mechanical properties of epoxy composites, such as polyimide,[34-35] polyhedral oligomeric silsesquioxane (POSS),[36-37] graphene,[38-40] carbon nanotubes (CNT),[41-42] etc. However, these additives are not well integrated into the epoxy matrix as a part of the polymer network. The addition of these additives may also interfere with the electrical properties, viscosity and adhesion strength of epoxy, which limits further applications in molding compounds. In this sense, current epoxy materials raise concerns for the high temperature operation of electronics.[43-46] Therefore, development of new generation of encapsulation materials with improved thermal properties is essential to keep pace with the ever-evolving market.

Cyanate ester are a family of monomers with reactive cyanate end groups (-OCN), which can form cyanurate network via trimerization through a step-growth process. It can be utilized in electronic packaging and aerospace applications due to excellent material properties, including low dielectric loss, good adhesion to metal, and the capability to work under high temperature.[47] It is reported that cyanate ester has a high thermal degradation temperature above 400 °C in nitrogen because of the thermally stable *s*-triazine structures.[48] Although cyanate ester possesses these advantages, there are few reports on combining cyanate ester with epoxy structures to develop molding compounds. Toldy *et al*.[49] worked on the reaction between phosphorous containing diglycidyl ether of bisphenol A with novolac type cyanate ester to form flame retarded blends. Lin and Liang *et al.* [50-51] tuned the hybrid epoxy cyanate esters structures to improve flame

retardancy and polymer processability. Despite these research efforts, the development of cyanate ester and epoxy copolymer system (CE/EP) for high glass transition temperature (T_g) and thermal stability have not been systematically investigated. The high temperature degradation mechanism of CE/EP was not well discussed. It is necessary to control the reactions in CE/EP and optimize its thermal properties for high temperature applications. Moreover, it is very important to consider the effect of several key factors, such as moisture, temperature and aging atmosphere, on the evolution of material properties for a more comprehensive evaluation of CE/EP copolymers.

In this chapter, cyanate ester and epoxy copolymers were developed with significant increase in T_g via controlled formulations. The relationship between chemical structures and thermal properties were investigated. Aging tests under elevated temperature and high humidity were conducted to evaluate the long term thermal stability of the CE/EP copolymers. The evolution of the structural changes for CE/EP resin has been monitored by IR characterization to reveal the degradation mechanism of CE/EP. Moisture induced degradation of polycyanurate network in CE/EP was proposed and verified as the main reason for thermal degradation. This manuscript provided new aspects in the study of modified epoxy network and evaluated the potential application of CE/EP copolymers in molding compounds for electronic packaging. Detailed and systematic analyses for the optimization of CE/EP system were presented.

2.2 Experimental Section

2.2.1 Materials

Bisphenol A cyanate ester, 2, 2-Bis(4-cyanatophenyl)propane, was supplied by AK Scientific. Tetra methyl biphenyl epoxy with an epoxide equivalent weight of 197 was supplied by Mitsubishi Chemical Corporation. Curing catalyst, aluminum acetylacetonate, was supplied by Aldrich Chemical Company, Inc. Curing agent, hexahydro-4-methylphthalic anhydride (HMPA), was supplied by Lindau Chemicals, Inc. Chemical structures of epoxy, cyanate ester, curing catalyst and curing agent for epoxy used in the experiments are shown in Scheme 2.1.

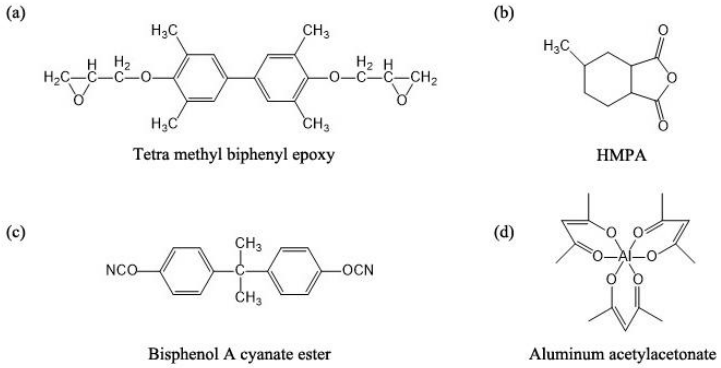

Scheme 2.1 – Chemical structures of (a) tetra methyl biphenyl epoxy (b) HMPA (c) bisphenol A cyanate ester and (d) aluminum acetylacetonate

2.2.2 Preparation of CE/EP

Epoxy was first melted at 110 ℃. Different ratios of cyanate ester were mixed with the molten epoxy under continuous stirring until a homogeneous yellow mixture was obtained. 0.3% of aluminum acetylacetonate was added to the mixture under stirring. The molar ratios of cyanate ester to epoxy were 1:3, 1:2, 1:1, 2:1 and 3:1, marked as CE/EP-

13, CE/EP-12, CE/EP-11, CE/EP-21 and CE/EP-31 respectively (Table 2.1). Samples were cured at 130 ℃ for 1 h, 170 ℃ for 1 h and 230 ˚C for 2 h as shown in Scheme 2.2. Neat epoxy and neat cyanate ester samples as references were prepared using the same curing procedure. The curing agent used in the epoxy reference samples was HMPA.

Table 2.1 – Composition of CE/EP copolymer

Components	Biphenyl epoxy (%)	Bisphenol A cyanate ester (%)
CE/EP-13	25	75
CE/EP-12	33	67
CE/EP-11	50	50
CE/EP-21	67	33
CE/EP-31	25	75

*Catalyst: 0.3 wt. %

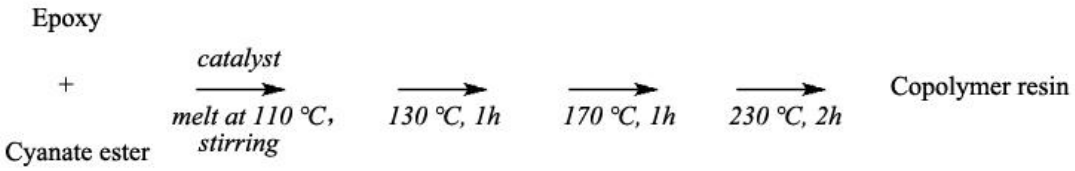

Scheme 2.2 – Schematic representation of sample preparation

2.2.3 Characterization of CE/EP

Differential scanning calorimetry (DSC Q2000, TA Instruments) was used for curing profiles. In the dynamic curing experiments, uncured samples of approximately 10 mg were ramped from 40 ℃ to 350 ℃ at 10 ℃/min under nitrogen atmosphere. In the isothermal curing experiments to profile the curing conversion, uncured samples were kept at 200 ℃, 210 ℃ and 220 ℃ for up to 60 min. Curing conversion α_{DSC} can be calculated according to the following equation:

$$\boldsymbol{\alpha_{DSC} = \frac{\Delta H_t}{\Delta H_{total}}} \qquad \textbf{(1)}$$

Where ΔH_t is the exothermic peak area with the function of time in an isothermal test, and ΔH_{total} is the total exothermic peak area from dynamic scan. Thermogravimetric analysis (TGA Q50, TA Instruments) was performed under nitrogen atmosphere. Cured samples were heated from 30 ℃ to 600 ℃ with a ramping rate of 10 ℃/min. Dynamic mechanical analysis (DMA Q800, TA Instruments) was used to determine the T_g. Specimens of rectangular shape with dimension of 15 mm × 10 mm × 5 mm were prepared. DMA tests were conducted in single cantilever mode, ramping 3 ℃/min to 300 ℃ at an oscillation frequency of 1 Hz. The strain magnitude was 10 μm. The melt viscosity was obtained by a Rheometer (Discovery HR-2 hybrid rheometer, TA Instruments). Uncured samples were kept at 110 ℃ between two parallel aluminum plates with diameter of 25 mm and tested using oscillation temperature sweep program with a temperature step of 5 ℃ and a frequency of 1 Hz. The strain was controlled at 0.5%. Dielectric constants and dielectric loss factors were obtained on an Agilent E4991A RF Impedance/Material Analyzer. The frequency was tested from 1 MHz to 100 MHz under

room temperature. Fourier transform infrared spectra (FTIR) were obtained on a Thermo Scientific iS50 FT-IR spectrometer using a diamond ATR mode. Specimens were scanned from 4000 cm^{-1} to 600 cm^{-1} with a resolution of 1 cm^{-1}.

In aging tests, cured samples were kept at 200 ℃ under air atmosphere in an oven for 21 days. The weight loss, chemical structure variation, thermal properties changes were characterized by gravimetric measurement, FTIR measurement and DMA measurement, respectively. In moisture absorption study, specimens were prepared with homogeneous thickness of approximately 1.3 mm and dried in a vacuum oven for 24 hours. Specimens were immersed in boiling water and taken out for weighing at intervals. The surfaces of the specimens were wiped dry before weighing. The weight changes were monitored by an OHAUS EP64C Explorer Pro analytical balance with a reliability of 0.1 mg. Water absorption M_t, as a function of time, can be calculated according to the following equation:

$$\boldsymbol{M_t = \frac{W_t - W_0}{W_0} \times 100\%} \qquad \textbf{(2)}$$

Where W_t is the wet weight of a specimen at time t and W_0 is the dry weight of the specimen.

2.3 Results and discussion

2.3.1 Chemical Reactions in CE/EP

Controlled curing reactions play a critical role in determining the chemical structures as well as corresponding properties of the CE/EP copolymers. For the copolymer system, a series of reactions can occur, which raises increasing difficulty for

the understanding of reaction mechanisms. As shown in Scheme 2.3, cyanate ester can form *s*-triazine structures via trimerization. Cyanate ester can also copolymerize with epoxy, by epoxide insertion and formation of oxazolidinone. Ring rearrangement and ring reformation can take place in the copolymer system as well.[52]

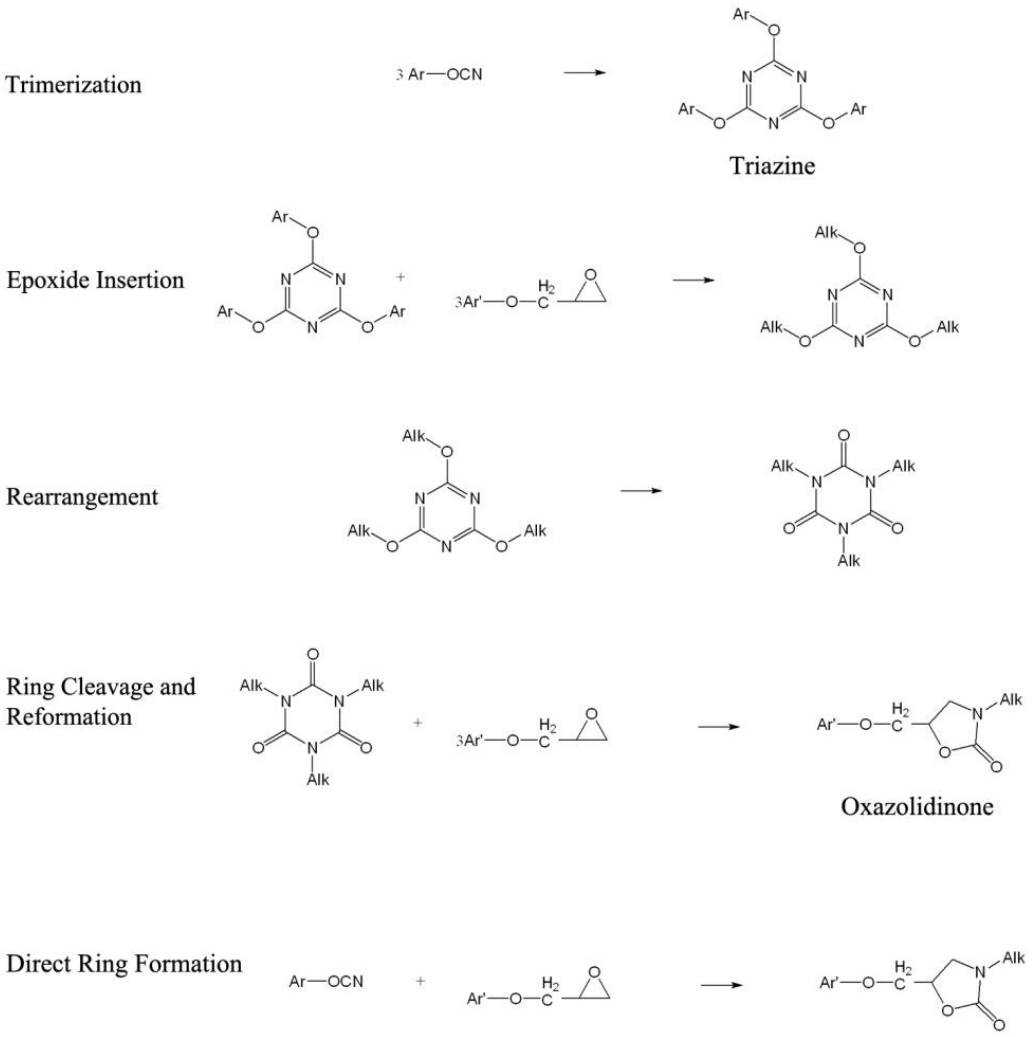

Scheme 2.3 – Reactions between cyanate ester and epoxy[53-54]

FTIR was taken to illustrate the chemical structure of CE/EP copolymer. As shown in Figure 2.1, the FTIR absorption peaks at 1556 cm^{-1} and 1360 cm^{-1} indicated the formation of triazine in CE/EP system. The absorption at 1747 cm^{-1} for oxazolidinone

was also observed. With the cyanate ester amount increasing in the formula, more triazine structures appeared while less oxazolidinone was formed. The absorption peaks at 1692 cm^{-1} was attributed to isocyanurate formed via rearrangement of triazine rings after epoxide insertion. Figure 2.2a shows DSC scans of uncured CE/EP samples. The main exothermic peak at 220 ℃ may be corresponding to the copolymerization reactions. The shoulder peak around 190 ℃, becoming more obvious with the increasing amount of cyanate ester in the mixture, may be corresponding to the trimerization reaction of cyanate ester since neat cyanate ester exhibited the curing peak temperature at 195 ℃ (Figure 2.3). This assumption can be further verified in the study of curing conversion, where the mixtures were cured isothermally at 220 ℃, 210 ℃ and 200 ℃. The degree of curing under each temperature is shown in Figure 2.2(b-d). After reaction for 40 min, the curing conversion of CE/EP-13 was 72.2% when cured at 200 ℃, compared to 99.6% when cured at 220 ℃. This difference in conversion between these two curing temperature can be attributed mainly to the formation of oxazolidinone that started to react at a higher temperature. As for CE/EP-12, the curing conversion at 200 ℃ was similar to that at 210 ℃, both of which were around 90%. The curing conversion of CE/EP-31 was above 95 % under all three different temperature conditions after 20 min, suggesting that the trimerization of cyanate ester was a dominant reaction in CE/EP-31 and it took place at a temperature lower than 200 ℃. The DSC results suggested that the trimerization of cyanate ester occurred first as a lower temperature, and then followed the copolymerization reactions mainly via epoxy insertion and the formation of oxazolidinone.[55] The addition of aluminum acetylacetonate catalyst could dramatically reduce the curing temperature of CE/EP copolymers as observed by DSC curves. The

peak temperature of the exothermic reaction for CE/EP-13 was reduced from 283.15 ℃ to 221.35 ℃ with catalyst added (Figure 2.4).

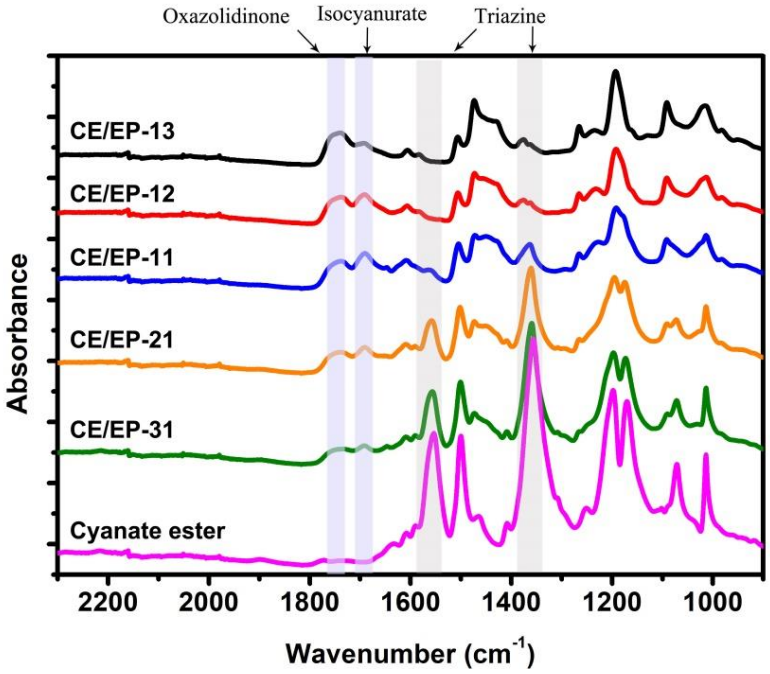

Figure 2.1 – FTIR spectra of CE/EP copolymer

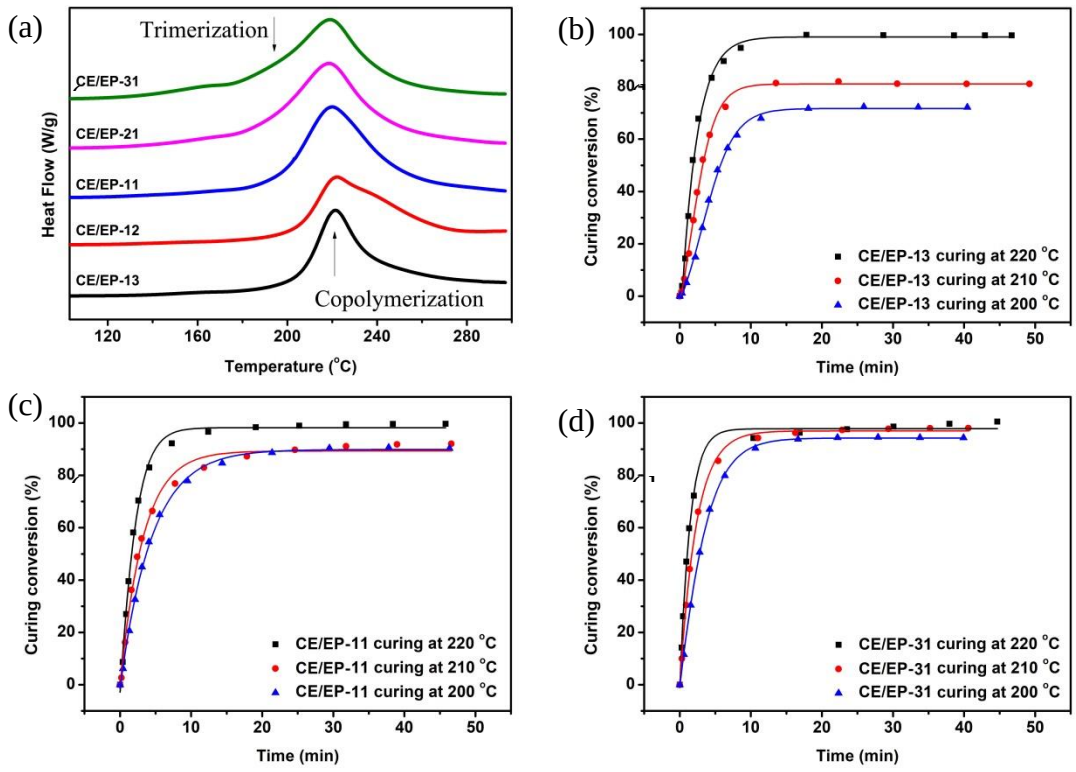

Figure 2.2 – (a) DSC scans of uncured CE/EP samples, and curing conversion of (b) CE/EP-13 (c) CE/EP-11 and (d) CE/EP-31 under different temperatures

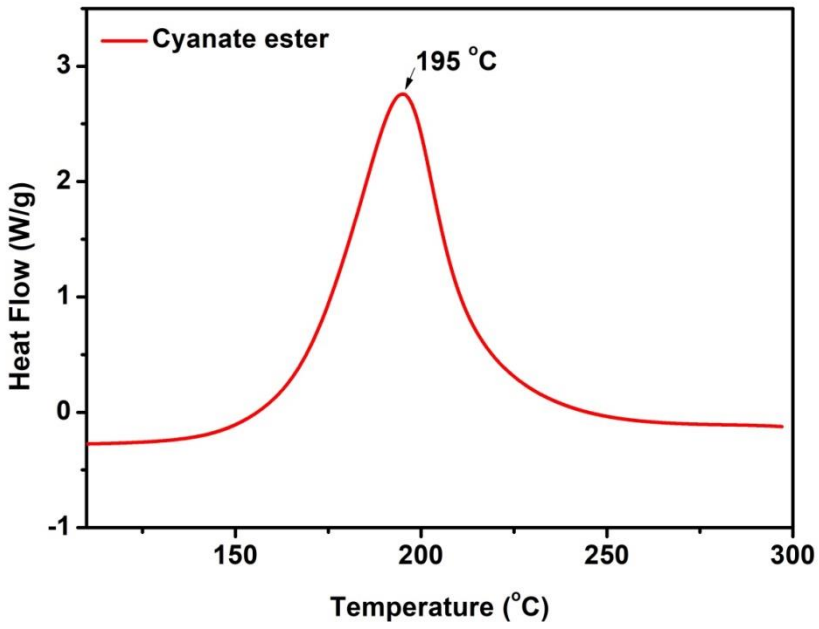

Figure 2.3 – DSC scan of cyanate ester

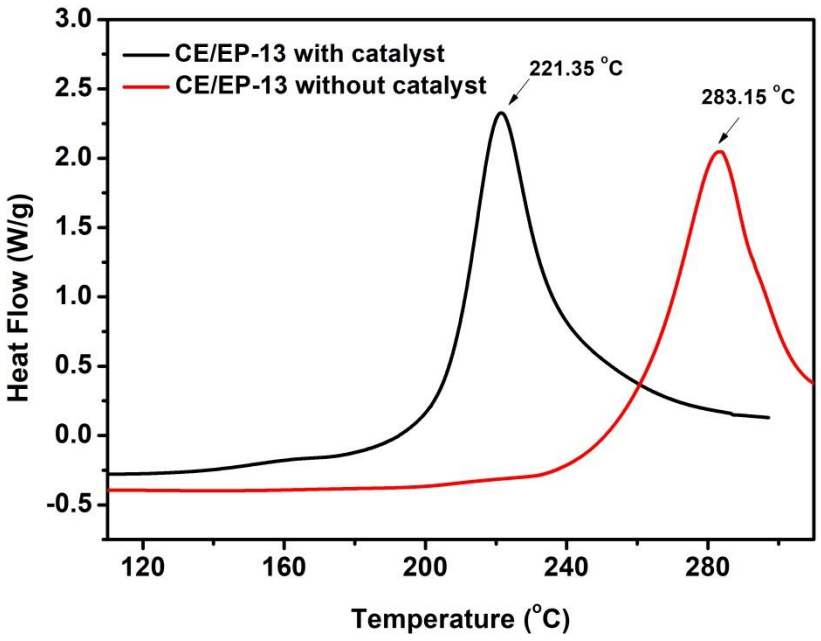

Figure 2.4 – DSC scans of CE/EP-13 with and without catalyst

2.3.2 Viscosity of CE/EP

For typical epoxy molding compounds, a polymer matrix is required to have an ideally low viscosity for good processability, since the filler loading usually can reach 70 - 90%.[28] Therefore, the viscosity of CE/EP was evaluated as an important factor for further applications. Figure 2.5 shows the viscosity of the CE/EP blends. The viscosity was approximately 0.1 Pa·s for uncured, molten blends, suggesting that the cyanate ester to epoxy ratio would not significantly affect the melt viscosity. The low viscosity of CE/EP blends prepared in this work was comparable to that of a typical biphenyl epoxy matrix (Figure 2.6). The drastic increase in viscosity around 170 ℃ to 190 ℃ indicated the beginning of curing reactions. Generally, blends with the more cyanate ester contents cured at the lower temperature, which was consistent with the DSC studies presented earlier.

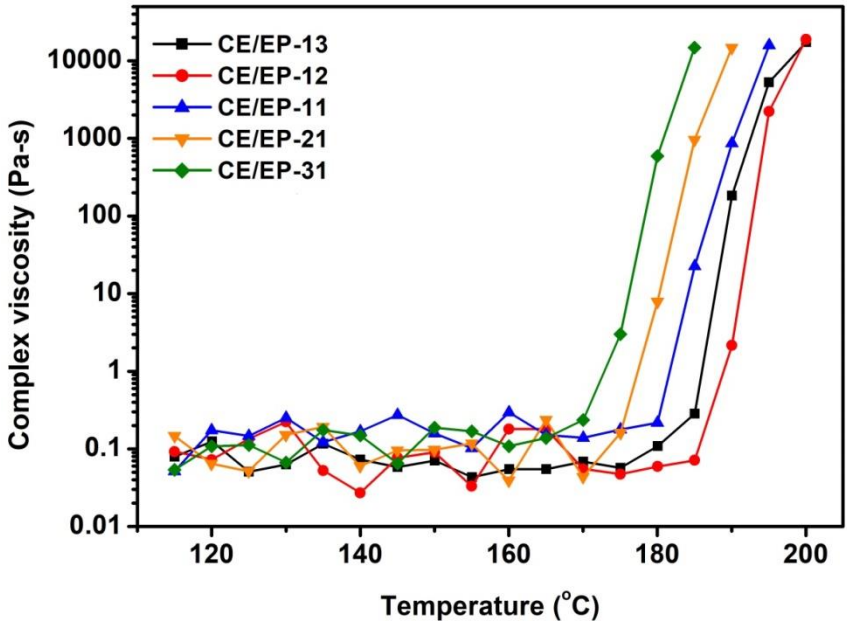

Figure 2.5 – Viscosity of CE/EP at different temperatures

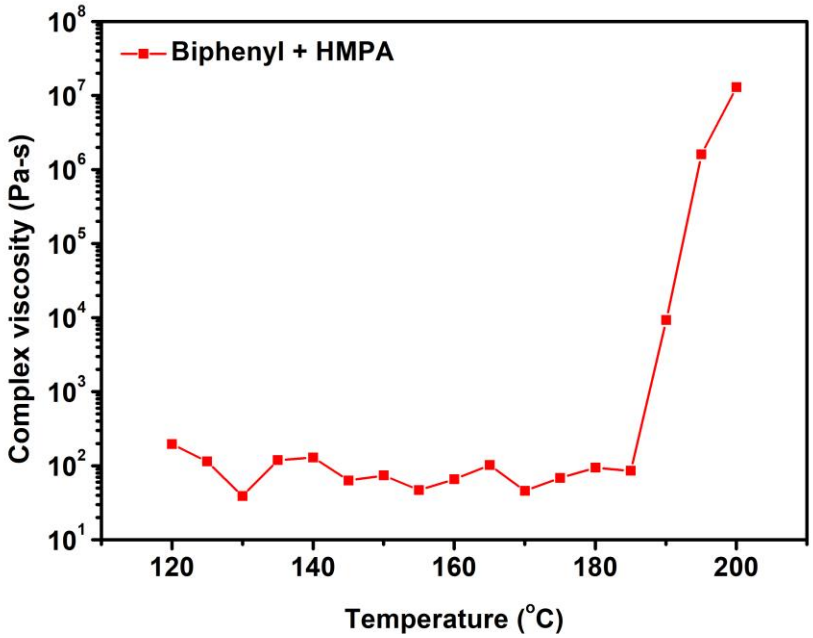

Figure 2.6 – Viscosity of biphenyl epoxy with HMPA hardener at different temperature

2.3.3 Dielectric properties of CE/EP

Molding compounds need to work under high dielectric stress in power devices, which makes low dielectric constant and low loss a prerequisite.[56] The dielectric properties of CE/EP are studied and listed in Table 2.2. Neat cyanate ester has the least dielectric constant and loss factor. With the increasing amount of cyanate ester in the resin, the dielectric constant decreased gradually. Therefore, the incorporation of cyanate ester in epoxy matrix helped lower the dielectric constant of epoxy matrix and thus provided better dielectric properties.

Table 2.2 – Dielectric properties of CE/EP*

Specimens	1 MHz		10 MHz		100 MHz	
	Dielectric constant	Loss factor	Dielectric constant	Loss factor	Dielectric constant	Loss factor
CE/EP-13	3.36	0.018	3.03	0.017	2.94	0.011
CE/EP-12	3.25	0.020	2.93	0.018	2.89	0.011
CE/EP-11	2.91	0.021	2.92	0.016	2.85	0.0052
CE/EP-21	2.73	0.017	2.72	0.0099	2.68	0.0042
CE/EP-31	2.68	0.022	2.68	0.0095	2.64	0.0036
Cyanate ester	2.45	0.012	2.28	0.0065	2.29	0.0018

*Test was conducted under room temperature.

2.3.4 Thermal Properties of CE/EP

It is important to determine the relationship between chemical structures and thermal stability for the design of molding compounds working at high temperature conditions. To evaluate the thermal stability of CE/EP copolymers, T_g is an important property that indicates the range of working temperature for polymers. As shown in Figure 2.7a, T_g indicated by tan delta in DMA test increased with the increase of cyanate ester ratio. For CE/EP-13 and CE/EP-12, the T_g were 200 ℃ and 212 ℃, respectively. T_g went up dramatically for CE/EP-11. However, this increasing trend slowed down for CE/EP-21 and CE/EP-31. The T_g of CE/EP-21 and CE/EP-31 were 271 ℃ and 275 ℃, respectively, and the T_g of neat cyanate ester was 288 ℃. The results indicated that cyanate ester promoted the increase of the T_g of resins significantly via the formation of triazine structures. In the meantime, the increase became less remarkable when it was approaching the T_g of neat cyanate ester. The intensity of tan delta peak of the resin is corresponding to the damping property. Damping increased with the formation of hydrogen bonding by epoxy segments. On the other hand, more cyanate ester increased the crosslinking density of the resin and therefore increased the damping as well. With the combination of these two factors, damping decreased first from CE/EP-13 to CE/EP-11 because of the decreased amount of epoxy segments and then increased from CE/EP-11 to CE/EP-31 because of the increased crosslinking density.

Figure 2.7b shows the thermal degradation behavior of CE/EP copolymers under nitrogen. All the thermal properties tested are listed in Table 2.3. $T_{5\%}$ and $T_{10\%}$ increased with the amount of cyanate ester. However, even the highest $T_{10\%}$ of CE/EP was about 30 ℃ lower than that of neat cyanate ester, suggesting that the starting temperature of

thermal degradation was largely determined by the epoxy part in the copolymer network. CE/EP-31 had a char yield of over 30% at 600 ℃ while CE/EP-13 was only 12.51% left. The significant increase in the char yields represented better heat resistance contributed by the triazine structures. In comparison, the T_g of epoxy control was 207 ℃ and the char yield at 600 ℃ was merely 7.5% (Figure 2.8). Therefore, cyanate ester helped to increase T_g and heat resistance of epoxy matrix effectively.

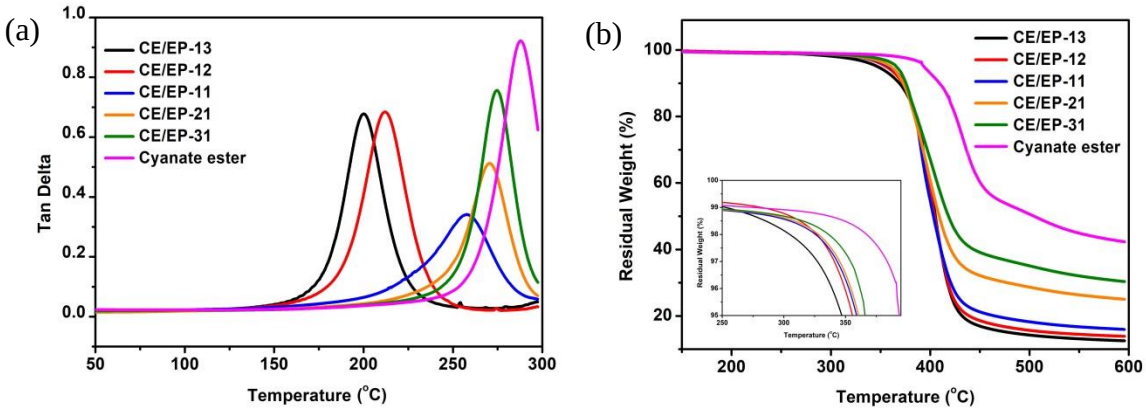

Figure 2.7 – Thermal properties of CE/EP copolymers (a) DMA tan delta of CE/EP (b) TGA curves of CE/EP

Table 2.3 – Thermal properties of resins with different cyanate ester to epoxy ratio*

Specimens	T_g (℃)	$T_{5\%}$ (℃)	$T_{10\%}$ (℃)	Char yields at 600 ℃ (%)
CE/EP-13	200	347	369	12.51
CE/EP-12	212	356	372	13.85
CE/EP-11	258	359	373	15.95
CE/EP-21	271	361	373	25.02

Table 2.3 continued

CE/EP-31	275	366	376	30.33
Cyanate ester	288	394	409	42.31

*$T_{5\%}$: 5% weight loss temperature, $T_{10\%}$: 10% weight loss temperature

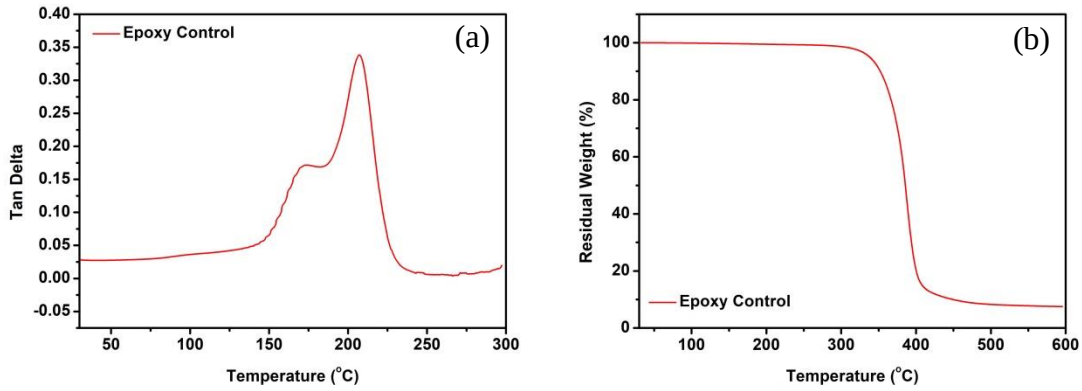

Figure 2.8 – Thermal properties of epoxy control (a) DSC scan of epoxy resin (b) TGA scan of epoxy resin.

2.3.5 High temperature aging mechanism and moisture absorption

The degradation mechanism of the CE/EP network was investigated by high temperature aging and moisture absorption tests. Figure 2.9 shows the chemical structure changes of CE/EP during aging tests by FTIR. In Figure 2.9a, the intensity of absorption peak around 3500-3200 cm^{-1} which is corresponding to phenolic –OH increased within 48 h, suggesting the formation of phenol groups through hydrolysis. Absorbance at 1692 cm^{-1} increased gradually over time, indicating the formation of isocyanurate via rearrangement (Figure 2.9b). The broaden peaks of CE/EP-13 around 1700 cm^{-1} after aging for 192 h and 336 h were corresponding to carbonyl groups (C=O) formed (Figure

2.9c). The carbonyl structures were formed via oxidation during aging at elevated temperature. Compared to CE/EP-13, CE/EP-31 showed improved chemical stability at high temperature and more triazine structures remained after aging at 200˚C (Figure 2.9d). However, copolymers with more cyanate ester showed larger mass loss during aging test (Figure 2.10a). Both neat cyanate ester and CE/EP-31 exhibited outgassing and blisters after aging for 504 h, while resins with less cyanate ester such as CE/EP-13 didn't show such problems (Figure 2.10 b-g). The T_g of CE/EP-31 decreased from 275 ℃ to 185 ℃ after aging for 336 h. The T_g drops of CE/EP-21 and CE/EP-11 were 60 ℃ and 48 ℃ after aging, respectively. For CE/EP-13 and CE/EP-12, the T_g were kept almost the same after aging (Table 2.4).

Generally, typical epoxy resins are subject to oxidation and chain scission during aging, which leads to the formation of carbonyl groups including ketone and ester[31-32, 45]. Triazine structure is more thermally stable compared to epoxy and does not decompose until the temperature reaches 450 ℃ in N_2.[48] However, it is reported that polycyanurate, which is the network formed by cyanate ester, may fail via hydrolysis under long time aging at temperature above 200 ℃.[47, 57] A typical hydrolysis reaction of polycyanurate is shown in Scheme 2.4,[58] where volatile products including CO_2 and NH_3 are formed. The volatile products formed through hydrolysis may be the main cause of blisters of neat cyanate ester and CE/EP-31. The formation of phenol groups according to Scheme 4 was observed in FTIR as well (Figure 2.9a). Cyanate ester residues can also absorb moisture in atmosphere and form carbamate, leading to outgassing of carbon dioxide above 200 ℃ (Scheme 2.5)[32]. However, there was few cyanate ester groups remained after curing

according to FTIR spectra shown in Figure 2.11, indicating that cyanate ester residues were not the cause of mass loss and blisters.

Therefore, according to results of thermal aging tests, CE/EP-12, CE/EP-11 and CE/EP-21 had better performance than other compositions since those three had less mass loss and blister, and still kept the T_g above 200 ℃ after aging tests. Considering the thermal properties discussed before, CE/EP-11 and CE/EP-21 were two of the best formulas providing high T_g and good thermal stability.

To evaluate the degradation performance and mechanism under high humidity, moisture absorption tests for CE/EP copolymers were conducted in boiling water. As shown in Figure 2.12, water uptake decreased with a decreasing molar ratio of cyanate ester, with the exception that the moisture absorption level of CE/EP-13 exceeded that of CE/EP-12 after 125 h. Moisture absorption of resin depends on the free volume in the cured polymer and the polarity of the chemical structures.[59-61] Micro-cracks generated in harsh environment like boiling water may have also contributed to the increasing amount of water absorbed. CE/EP-13 had a lower glass transition temperature and less heat stability compared to copolymers with other formulas and, therefore, may form micro-cracks after 125 h resulting in an increased water uptake. Moisture absorption of CE/EP-21 and CE/EP-31 increased again after 70 h, which may suggest the occurrence of hydrolysis reactions.

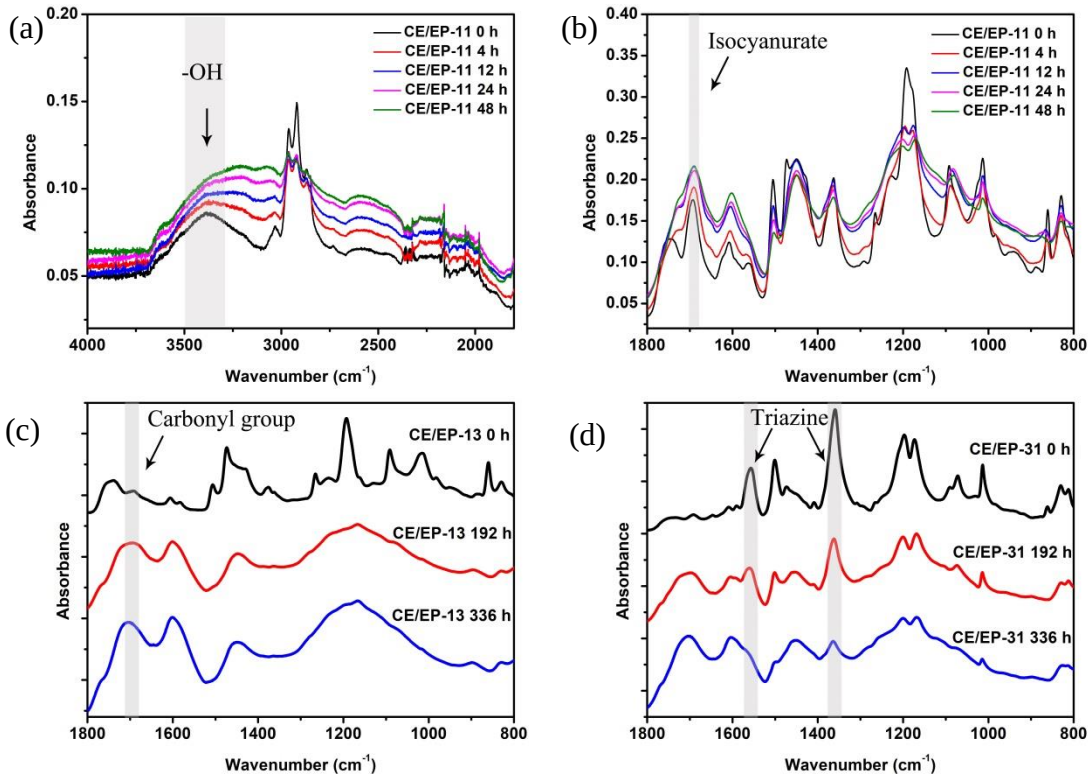

Figure 2.9 – FTIR aging spectra of CE/EP copolymers aged at 200 °C (a) short term aging spectra of CE/EP-11 from 4000 to 1800 cm^{-1} (b) short term aging spectra of CE/EP-11 from 1800 to 800 cm^{-1} (c) aging spectra of CE/EP-13 at 0 h, 192 h and 336 h (d) aging spectra of CE/EP-31 at 0 h, 192 h and 336 h.

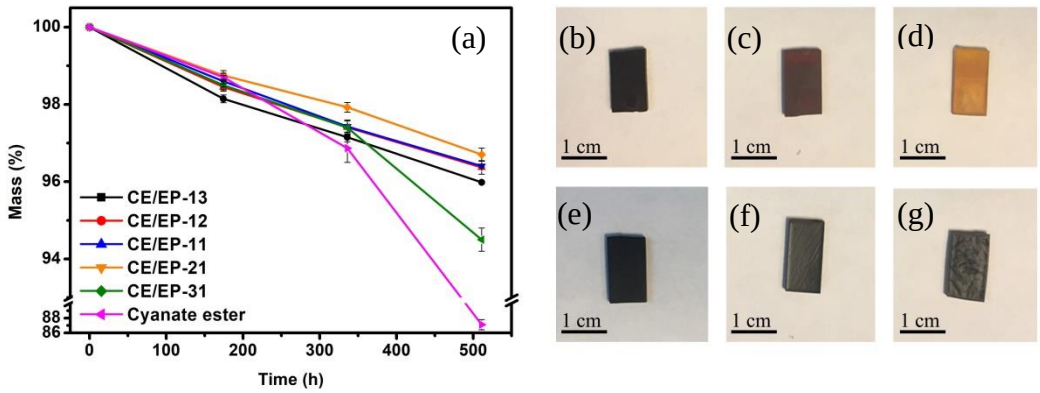

Figure 2.10 – (a) Mass loss of CE/EP during aging test and photographs of (b) CE/EP-13 before aging (c) CE/EP-31 before aging (d) Cyanate ester before aging (e) CE/EP-13 aging for 504 h (f) CE/EP-31 aging for 504 h (g) Cyanate ester aging for 504 h.

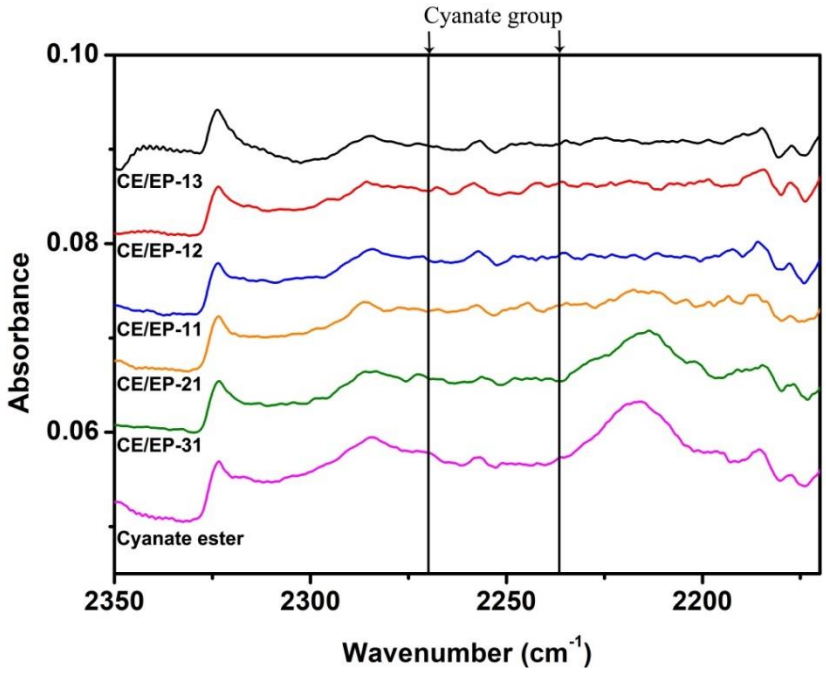

Figure 2.11 – FTIR spectra of CE/EP resin cured

Table 2.4 – Glass transition temperature change after aging test

	CE/EP-13	CE/EP-12	CE/EP-11	CE/EP-21	CE/EP-31
T_g (°C) as prepared	200	219	258	270	271
T_g (°C) aged 336 h at 200 °C	198	220	210	210	185

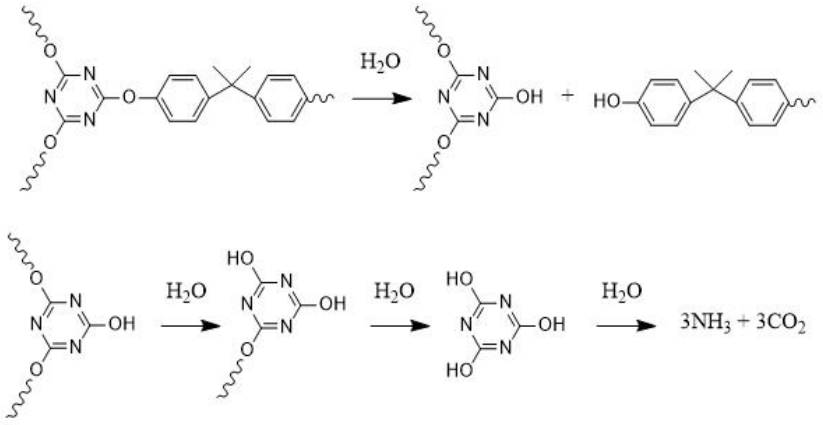

Scheme 2.4 – Possible hydrolysis reactions occurred[58]

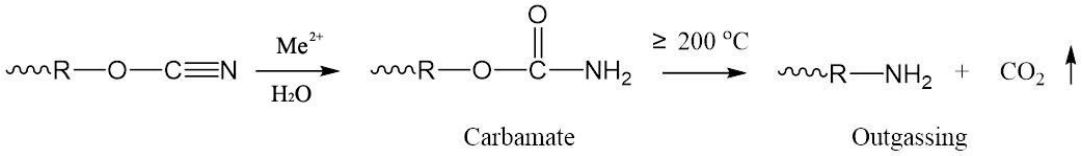

Scheme 2.5 – Hydrolysis of cyanate ester[47]

It is found that T_g may drop due to the plasticizing effect of water absorbed.[62-64] The moisture absorption trend was corresponding to the depressed T_g trend as shown in Table 2.4. Larger T_g depressions were observed for copolymers with higher moisture absorption. CE/EP-31 was proved to have the highest moisture uptake and suffered most from blistering among all CE/EP samples. The chemical structure changes of CE/EP-31 after immersion in boiling water for 1392 h was shown in Figure 2.13. Increase in the absorbance at 3338 cm^{-1} can be attributed to the formation of hydroxyl groups after hydrolysis (Scheme 2.4). This further confirmed the explanation of degradation mechanism due to hydrolysis of polycyanurate network. The increasing peak at 1693 cm^{-1} indicated the formation of isocyanurate which was also observed during aging tests,

suggesting that this rearrangement would happen over time. Chemical changes of other CE/EP samples after moisture absorption were shown in Figure 2.14 and no notable changes were observed.

From the above results, it was found that the T_g and degradation temperature of CE/EP copolymer increased with an increasing amount of triazine structures formed in the polymer network, with a maximum T_g of 275 ℃. However, polycyanurate network suffered from high water uptake and hydrolysis. CE/EP-31 performed worst among these CE/EP samples in aging mass loss. CE/EP-31 and CE/EP-21 exhibited largely depressed T_g after aging test because they absorbed more water than other samples. For CE/EP-13, it had the lowest T_g among these formulas, and thermo-oxidation via formation of carbonyl groups disturbed its original polymer network. CE/EP-12 and CE/EP-11 have comparable viscosity and dielectric properties. CE/EP-11 had the T_g as high as 258 ℃, while CE/EP-12 absorbed less moisture and had less drop in T_g after aging. Therefore, the CE/EP copolymer with 33%-50% cyanate ester moieties (between CE/EP-12 and CE/EP-11) was considered to be a desirable composition for molding compounds.

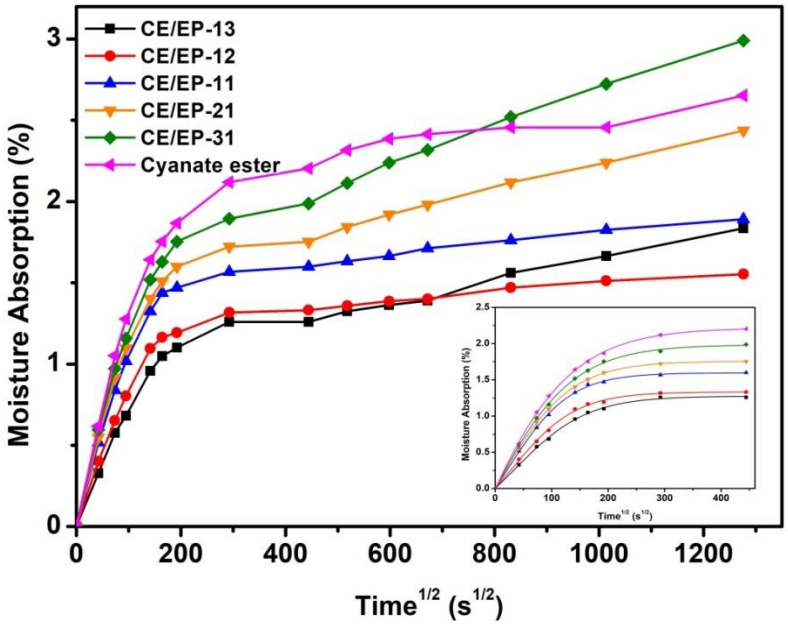

Figure 2.12 – Gravimetric measurement of water absorption in boiling water

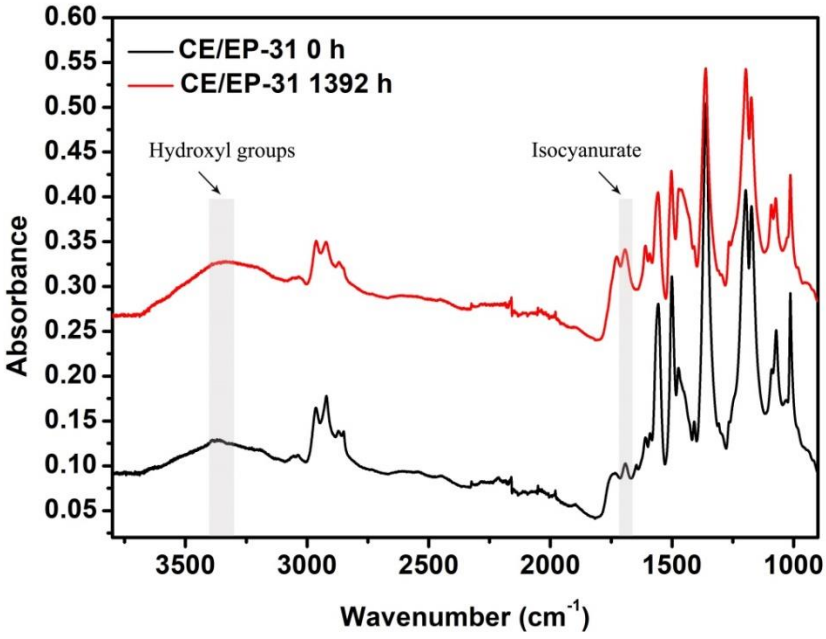

Figure 2.13 – FTIR spectra of CE/EP-31 before and after moisture absorption

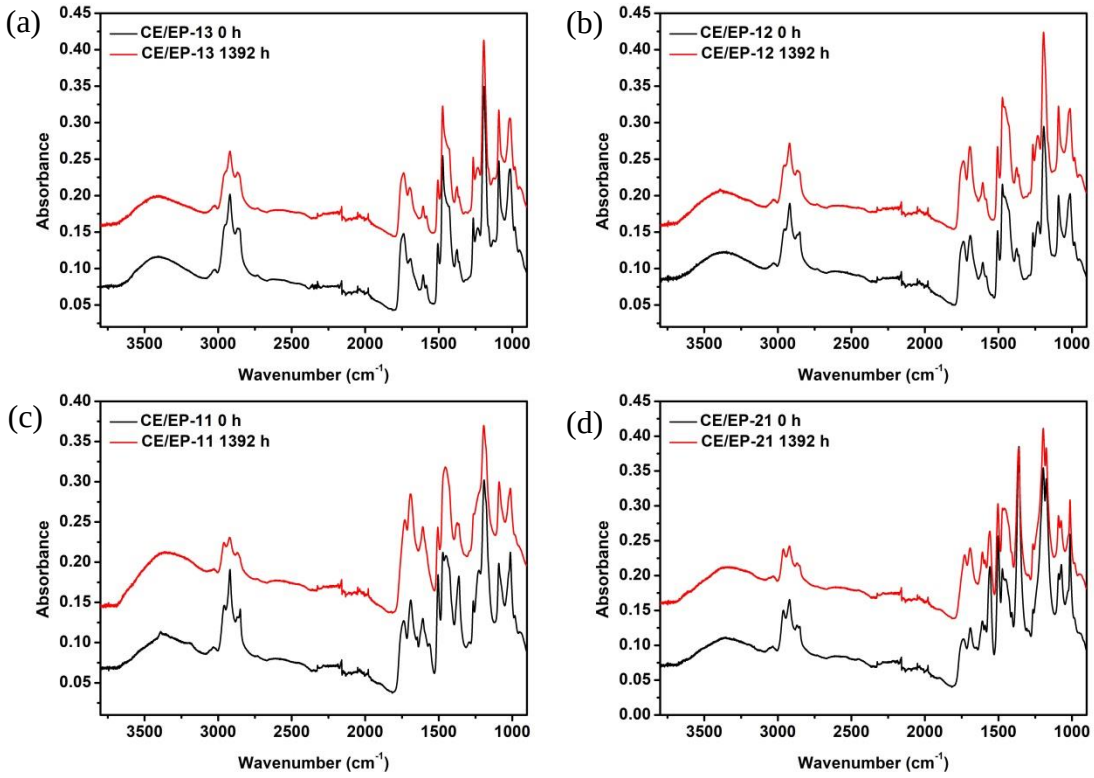

Figure 2.14 – FTIR spectra of (a) CE/EP-13 (b) CE/EP-12 (c) CE/EP-11 and (d) CE/EP-21 before and after moisture absorption test for 1392 h

2.4 Conclusion

In this chapter, a high temperature stable copolymer system based on cyanate ester/epoxy was developed and optimized. The curing reactions and thermal properties of CE/EP copolymers were characterized and studied by DSC, DMA, TGA and FTIR. The copolymer exhibited increased T_g with increased molar ratios of cyanate ester, and the maximum T_g can reach as high as 275 ℃. The melt viscosity of the copolymer blends was kept low around 0.1 Pa·s for all formulations, which provides the precondition for the further addition of fillers. During the aging tests, CE/EP system experienced thermo-oxidation via the formation of carbonyl groups and the rearrangement of cyanurate into isocyanurate. Although the increased amount of cyanate ester in the copolymer offered

higher T_g, surplus cyanate ester resulted in blisters on the cured materials, higher moisture absorption and hydrolysis of polycyanurate network. Therefore, the optimized composition of CE/EP should contain 33%-50% cyanate ester in the copolymer, where a balanced thermal property and aging performance can be achieved. The CE/EP copolymer developed exhibited great potential in the application of high temperature reliable molding compounds.

CHAPTER 3. POLYIMIDE INCORPORATED CYANATE ESTER/EPOXY COPOLYMER

The rapid development of high power devices has driven the requirement for high temperature stable epoxy molding compounds. In this chapter, a designed polymer blend system consisting of cyanate ester/epoxy copolymers modified by polyimide (CE/EP-PI) has been studied. CE/EP-PI resins showed outstanding long-term stability at high temperature with low mass loss and increased fracture toughness after aging at 200 ℃.

3.1 Background

The upsurge in high power and high density electronics inevitably raises increasing concerns in heat management and, therefore, imposes more stringent requirements on the high temperature stability of encapsulation materials. In addition, wide band gap (WBG) semiconductors, such as silicon carbide (SiC) and gallium nitride (GaN), are developing rapidly for high power and high frequency applications. These WBG semiconductors undergo a maximal junction temperature higher than 200 ℃, which is 50-100 ℃ higher than typical silicon devices.[65-66] Epoxy molding compounds (EMCs) are one of standard encapsulation materials in electronics packaging protecting the integrated circuit (IC) chip from chemical and physical attacks.[10] However, they still experience deterioration in thermal, mechanical and electrical properties under elevated temperature.[10, 29, 67] The material failure is mostly due to the thermo-oxidative degradation. The formation of carbonyl groups, bond breaking in the polymer networks and chain scission result in increased modulus and mass loss.[30-33] Therefore, it is essential to develop a new generation of molding compounds to meet the urgent demands of current high power

electronics industry. In the design and development of high temperature EMCs, glass transition temperature (T_g) and thermal stability have been used to evaluate their potential high temperature application.[68] With this criterion, efforts have been made to incorporate thermally stable chemical structures into epoxy networks by copolymerization, such as *s*-triazine rings,[69-70] poly (ether sulfone),[71-72] cyclic imide,[73] and so forth. Having focused on the effects of copolymerized chemical structures in epoxy, studies rarely look into the influence of physically tuned polymer structures, such as polymer blends. Well-designed polymer blends can also provide the epoxy system with an enhanced thermal stability. However, most polymer blends are immiscible due to the low entropy of mixing, which makes it challenging to develop a miscible polymer blends with homogeneous phase that can take advantages of both components. In this sense, it is worthwhile to develop an epoxy based polymer blend for high temperature application.

Aromatic polyimides are intensively used in high temperature applications for their excellent heat resistance.[12, 74-76] Highly aromatic polyimides generally have thermal degradation temperatures above 300 ℃ and T_g above 200 ℃, along with other properties such as good chemical resistance, strong mechanical properties, low thermal expansion coefficient and inherent flame combustion resistance.[12, 76-79] Having superior properties, polyimide can be incorporated into the epoxy based polymer to improve its performance. Lee and Wang synthesized an epoxy-polyimide based semi-IPN with high hydrolytic stability and good proton-transporting properties.[80] Jin *et al.* reported the toughness improvement of epoxy resin via the incorporation of a hyperbranched polyimide.[81] Baker *et al.* studied the enhancement of flexural strength and impact strength in epoxy resin with the addition of polyimide.[82] However, the improvement of thermal stability and T_g

of epoxy resin through polyimide incorporation has been rarely reported. Moreover, it is essential to systematically investigate the effects of thermal aging on the properties of epoxy/polyimide system, so as to evaluate its long term stability.

In this chapter, polyimide was incorporated into an epoxy and cyanate ester (CE/EP) copolymer system. The chemical and physical structures of polyimide incorporated CE/EP network was studied by thermal profiles and microscope images. The thermal and mechanical properties of this polyimide modified CE/EP system (CE/EP-PI) were investigated. Evaluation of the long term thermal stability of CE/EP-PI was conducted via high temperature aging and moisture absorption tests. In order to have an understanding of its property evolution at high temperatures, the changes in storage modulus, T_g and fracture toughness were characterized during aging tests. This paper demonstrated the potential of a novel polyimide modified CE/EP structure as molding compounds for high temperature applications.

3.2 Experimental Section

3.2.1 Materials

Tetra methyl biphenyl epoxy with an epoxy equivalent weight (EEW) of 197 was obtained from Mitsubishi Chemical Corporation. 2, 2-Bis(4-cyanatophenyl)propane was purchased from AK Scientific. Polyimide, Vespel SP-1, was obtained from DuPont (Table 3.1). Aluminum acetylacetonate, used as curing catalyst, was obtained from Aldrich Chemical Company. The chemical structures of polyimide， epoxy and cyanate ester used in this study are shown in Scheme 3.1.

Table 3.1 – Information of polyimide used in this work

Properties*	Polyimide
Flexural modulus at 260 °C (MPa)	1724
Dielectric constant at 10^6 Hz	3.55
Loss Factor at 10^6 Hz	0.0034

*Information obtained from data sheet provided by DuPont

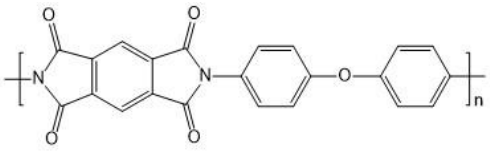

Polyimide, Vespel SP-1,

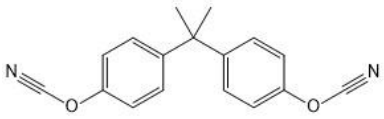

2-Bis(4-cyanatophenyl)propane

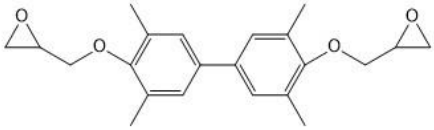

Tetra methyl biphenyl epoxy

Scheme 3.1 – Chemical structures of polyimide, epoxy and cyanate ester used

3.2.2 Preparation of CE/EP-PI

To prepare the polyimide modified resin, epoxy and cyanate ester were first melted at 110 °C with a molar ratio of 1:1. 0.3% aluminum acetylacetonate was added to the melt as curing catalyst. Different amounts of polyimide were added to the mixture under stirring. The polyimide contents and formula of each sample are listed in Table 3.2. The uncured samples were kept under stirring until polyimide completely dissolved in the

melt. The mixture was then cured at 130 ℃ for 1 h, 170 ℃ for 1 h, and finally kept at 230 ˚C for 2 h.

Table 3.2 – Formulas of CE/EP-PI samples

Sample Name	Cyanate ester : Epoxy	Polyimide content (wt. %)
CE/EP	1:1	0
CE/EP-5PI	1:1	5
CE/EP-10PI	1:1	10
CE/EP-15PI	1:1	15

3.2.3 Characterization of CE/EP-PI

The curing profiles of the resin samples were obtained by Q2000 differential scanning calorimetry (DSC, TA Instruments). Uncured samples were sealed in an aluminum pan and heated to 300 ℃ at a rate of 10 ℃/min under nitrogen. To obtain the fourier-transform infrared spectra (FTIR), Thermo Scientific iS50 was used in the diamond ATR mode, scanning from 4000 cm^{-1} to 600 cm^{-1} with a resolution of 1 cm^{-1}. The phase images were scanned by AFM (Bruker) in a tapping mode . Thermal degradation was characterized by Q50 thermogravimetric analyzer (TGA, TA Instruments), heating the cured samples from room temperature to 600 ℃ under nitrogen atmosphere. T_g and modulus of the modified resins were acquired by dynamic mechanical analysis (DMA, Q800, TA Instruments) using the single cantilever mode

with an oscillation frequency of 1 Hz. DMA tests were conducted from 30 to 300 ℃ at a rate of 3 ℃/min under nitrogen. The melt viscosity before curing was investigated by a Discovery HR-2 hybrid rheometer (TA Instruments), using 25 mm diameter parallel aluminum plates. The complex viscosity was obtained using an oscillation temperature sweep program at the frequency of 1 Hz. Agilent E4991A RF Impedance/Material Analyzer was used to obtain dielectric constants and loss factors of the resins from 10 MHz to 1 GHz at room temperature. The three point bending tests were conducted on an Instron 5548 MicroTester according to ASTM E-399. The fracture surfaces of modified resins were characterized by Hitachi SU8010 scanning electron microscopy.

For the long term stability tests, modified resins were kept at 200 ℃ in air atmosphere for up to 3 weeks. The mass loss was monitored by an OHAUS EP64C Explorer Pro analytical balance. The moisture absorption tests were performed by immersing cured resins in boiling water for ten days, and the weight was measured at intervals. Water absorption M_t was calculated based on the following equation.

$$M_t = \frac{W_t - W_0}{W_0} \times 100\% \qquad \textbf{(3)}$$

Where W_t represents the wet weight of a resin sample at time *t* and W_0 is the dry weight of the resin.

3.3 Results and Discussion

3.3.1 Structures of CE/EP-PI polymer network

In order to gain a comprehensive understanding of the network structure of CE/EP-PI, it is essential to investigate the reactions occurred in this system. The chemical

reactions in the formation of CE/EP polymer network include trimerization of cyanate ester, copolymerization of cyanate ester and epoxy, and other side reactions. The detailed reactions are shown in Scheme 3.2. *s*-Triazine structures are formed from three cyanate ester groups and can grow into a polycyanurate network, which provides enhanced thermal stability to the network structure.[57] Epoxide insertion further builds up the polymer network by attaching epoxy monomers into the polycyanurate network. Another important reaction is the direct ring formation of cyanate ester and epoxy, which forms an oxazolidinone ring and contributes to the formation of linear segments in this crosslinking structure.[83-84]

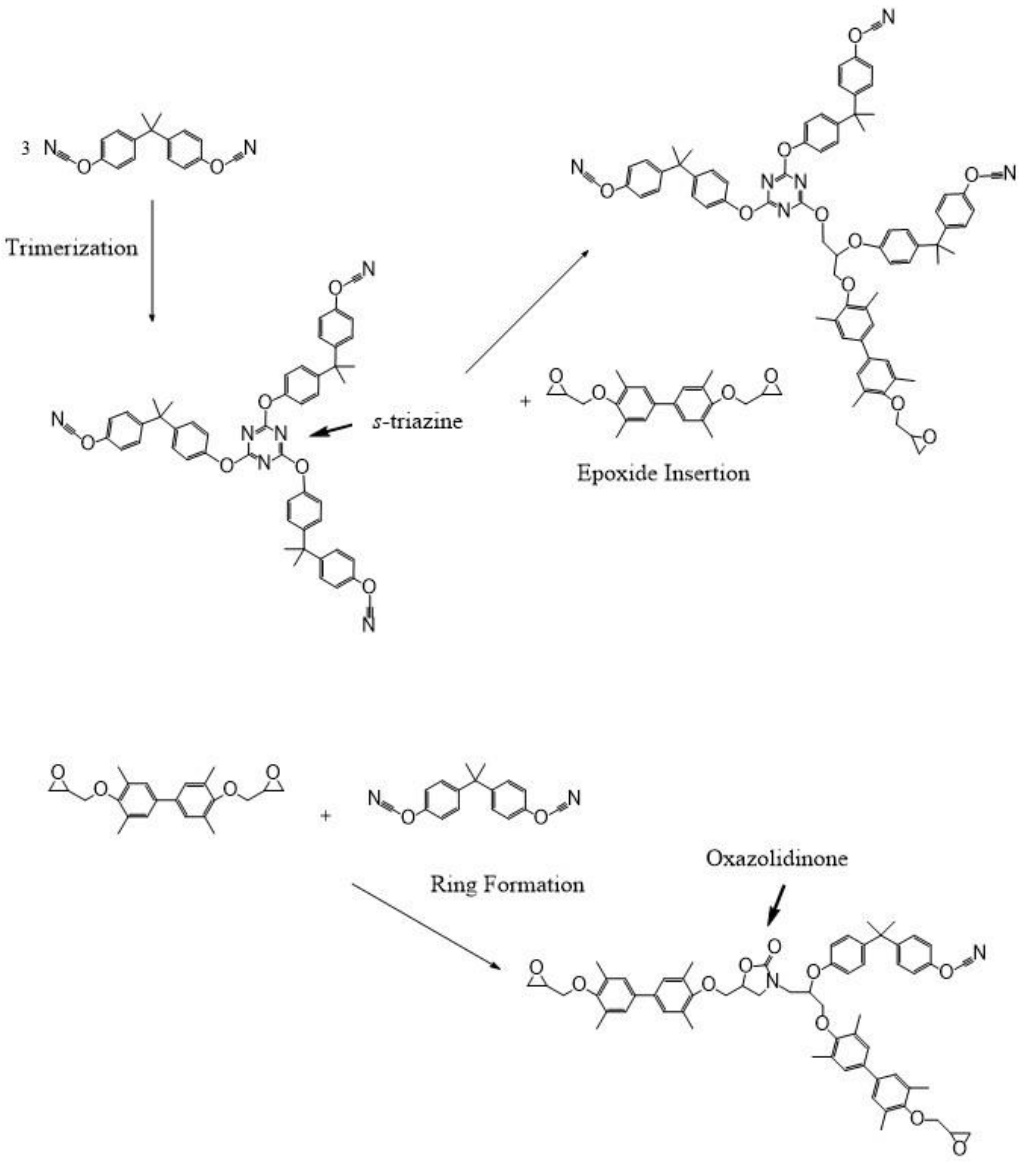

Scheme 3.2 – Reactions involved in the formation of CE/EP polymer network.

In CE/EP-PI, the cyanate ester and epoxy copolymer network was formed in the presence of polyimide. According to DSC plot (Figure 3.1), there was no extra exothermic peak observed other than the curing peak of the CE/EP. The normalized reaction enthalpy (ΔH*) according to the CE/EP mass is similar for the four samples with different polyimide loading, which suggested that polyimide was not involved in the CE/EP crosslinking reactions. However, the peak temperature shifted slightly to the

higher temperature, indicating that polyimide may somewhat hinder and slow down the reactions in the CE/EP system. FTIR scans of CE/EP-PI provided detailed information on the chemical structures in the cured copolymer (Figure 3.2). The absorption peaks of *s*-triazine groups were observed at 1559 cm^{-1} and 1363 cm^{-1}.[85] The absorption peaks at 1748 cm^{-1} and 1693 cm^{-1} were attributed to oxazolidinone and isocyanurate, respectively.[52] The absorption peak at 1713 cm^{-1} was corresponding to that of the imide carbonyl groups of polyimide, which increased gradually with the increasing ratio of polyimide in resins.[86-87] The FTIR spectrum of polyimide was shown in Figure 3.3 as a reference.

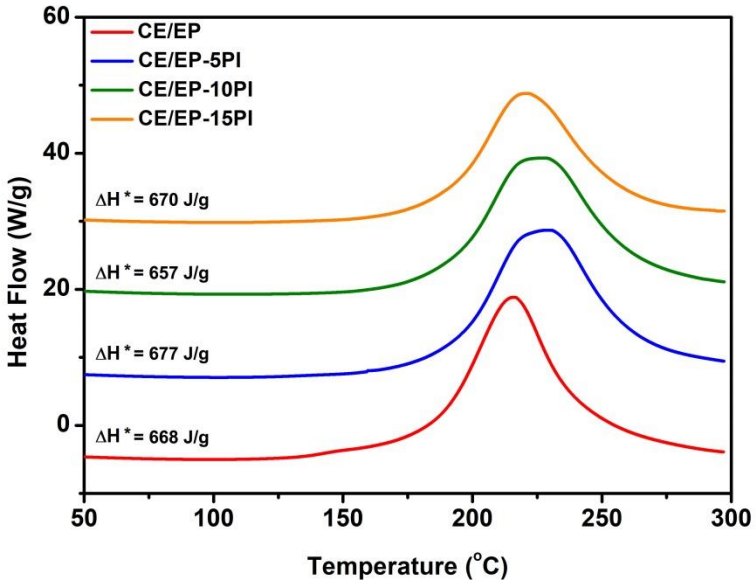

Figure 3.1 – DSC scans of CE/EP-PI (reaction enthalpy ΔH* is normalized to the mass of CE/EP).

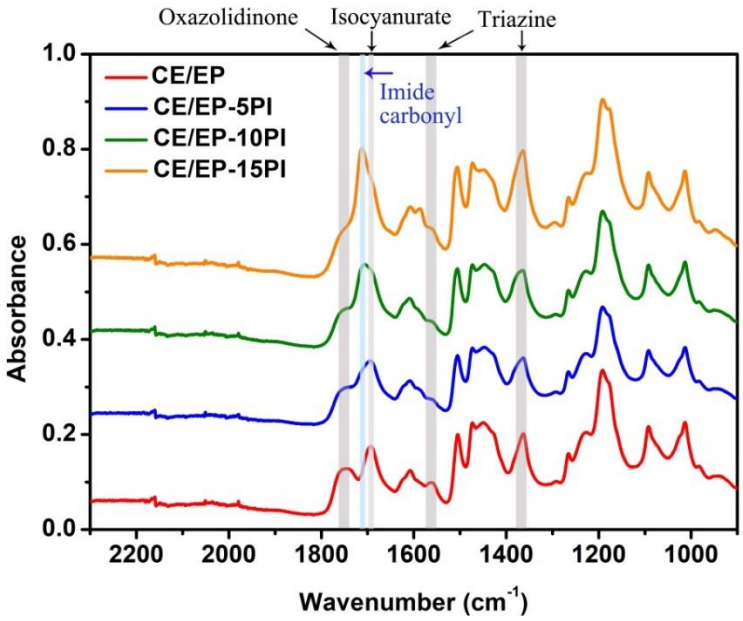

Figure 3.2 – FTIR spectra of CE/EP-PI.

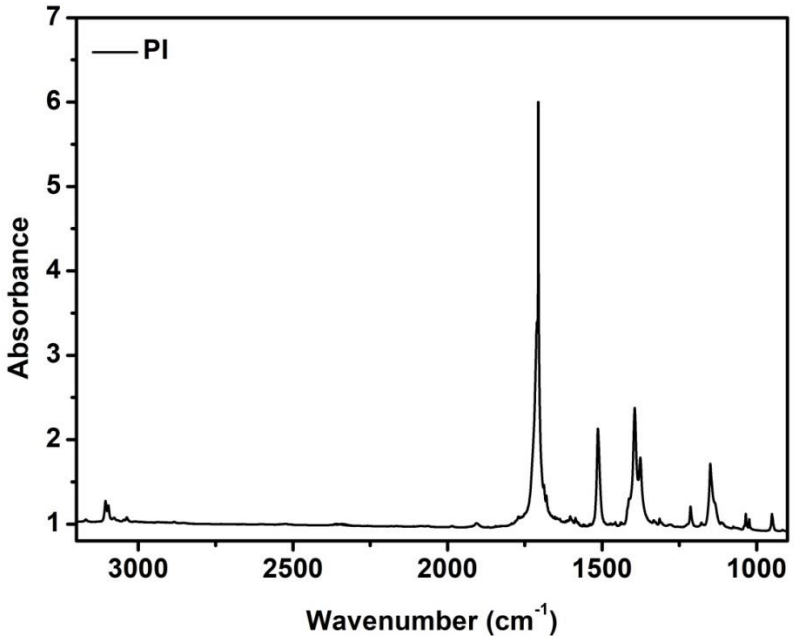

Figure 3.3 – FTIR spectra of Polyimide

The polyimide showed an excellent compatibility with CE/EP copolymer system (Figure 3.4) as an additive. The uncured melts of CE/EP-PI were transparent, indicating

that the polyimide was well dispersed in the melts. The cured resins with polyimide were slightly darker than the pure CE/EP, and exhibited a homogeneous pellet form similar to that of CE/EP. Generally, it is not thermodynamically favorable for the mixing of two different polymers with high level of uniformly because of the low entropy of mixing, which makes phase separation a common phenomenon in most polymer blends.[88] However, in the case of CE/EP-PI, both CE/EP and polyimide contained high contents of aromatic rings, and their similarity in chemical structure facilitated the association of the two parts. This association helped to improve the miscibility of this system and provided a homogeneous phase ultimately with 5% of polyimide loading (Figure 3.5a-b). However, with the increasing loading of polyimide, phase separation was observed under AFM (Figure 3.5c-d). Particularly, samples with 15% of polyimide loading exhibited fragmented structures with aggregated polyimide domains, which was typical in the evolution of phase separation.[89] The phase behavior would affect the properties of CE/EP-PI, thus it is important to control the loading amount of polyimide in the CE/EP network. The distribution of polyimide in CE/EP crosslinking network can be explained by Scheme 3.3. At a lower loading, the polyimide dispersed evenly in the copolymer matrix, while a second phase was formed by polyimide aggregation when increasing the polyimide loading.

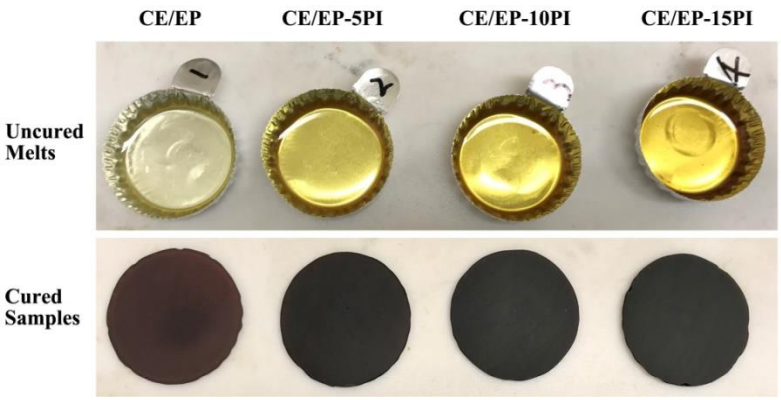

Figure 3.4 – Images of CE/EP-PI melts and cured resins

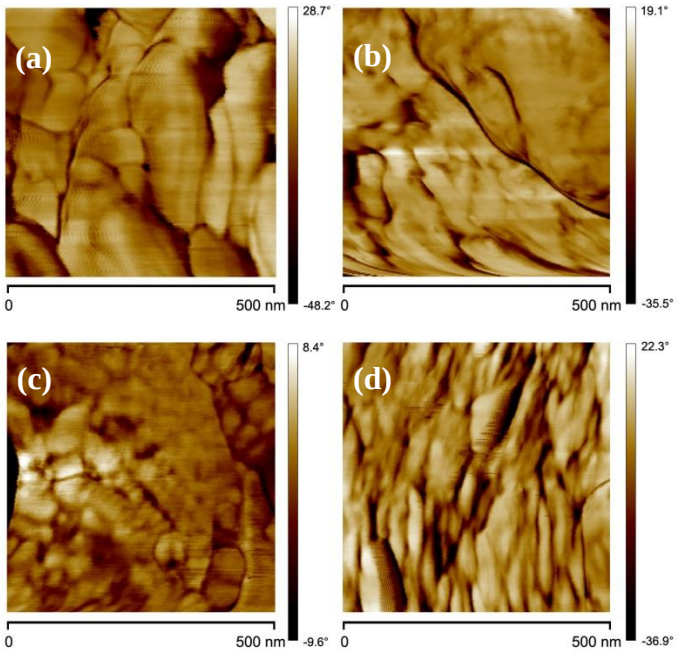

Figure 3.5 – AFM tapping phase images of (a) CE/EP (b) CE/EP-5PI (c) CE/EP-10PI and (d) CE/EP-15PI

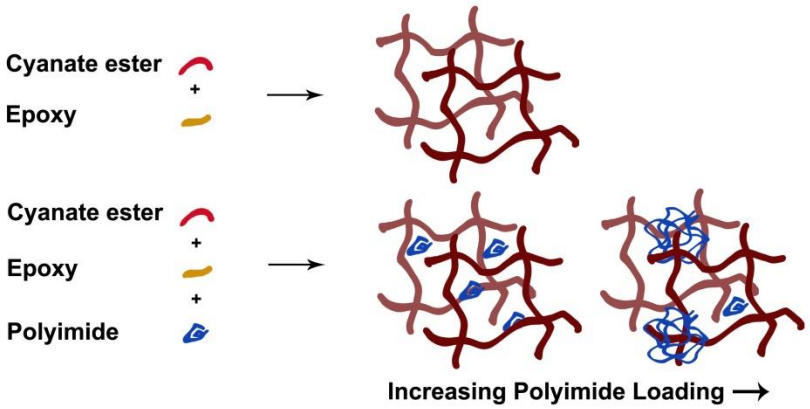

Scheme 3.3 – Incorporation of polyimide into CE/EP network

3.3.2 Properties of CE/EP-PI resins

Thermal properties including T_g and degradation temperature of CE/EP-PI were determined to investigate the effects of polyimide incorporation on the resins. It is shown that the T_g of the blend resin increased with the increase of polyimide loading in the resin (Figure 3.6a). The T_g increased from 257.8 ℃ to 270.5 ℃ upon 5% loading of polyimide. However, the T_g only showed a slight increase by 1.9 ℃ when polyimide loadings further increased from 10% to 15%, which suggested that the increase in T_g was not following a linear fashion. The increase in T_g may be explained by the decreased mobility of CE/EP chain segments after the addition of polyimide, in which polyimide can fill in free volume of CE/EP network structure. The formation of a denser network structure was also verified by the increase in resin density, as shown in Table 3.3. The density of CE/EP-PI increased from 1.192 g/cm^3 to 1.200 g/cm^3 with the polyimide loading increasing from 0 to 10%. However, the density decreased slightly to 1.198 g/cm^3 with 15% of polyimide added, suggesting that 15% of polyimide led to a looser network structure compared to CE/EP-10PI due to the aggregation of surplus polyimide.

The thermal degradation behavior of CE/EP-PI was studied by TGA. In TGA scans, CE/EP-PI had a larger residual weight at 600 ℃ compared to CE/EP since polyimide had a better high temperature resistance than CE/EP (Figure 3.6b). The derivative curve of weight loss indicated a similar degradation behavior of CE/EP both with and without polyimide, indicating that there was no chemical bonding between CE/EP and polyimide. The onset degradation temperature and the temperature for the maximum decomposition rate were around 325 ℃ and 392 ℃ respectively, which were not affected by the incorporation of polyimide. Therefore, the incorporation of polyimide increased the T_g and char yields via the formation of a denser network structure and excellent thermal resistance of polyimide, but not affecting the thermal degradation of CE/EP network.

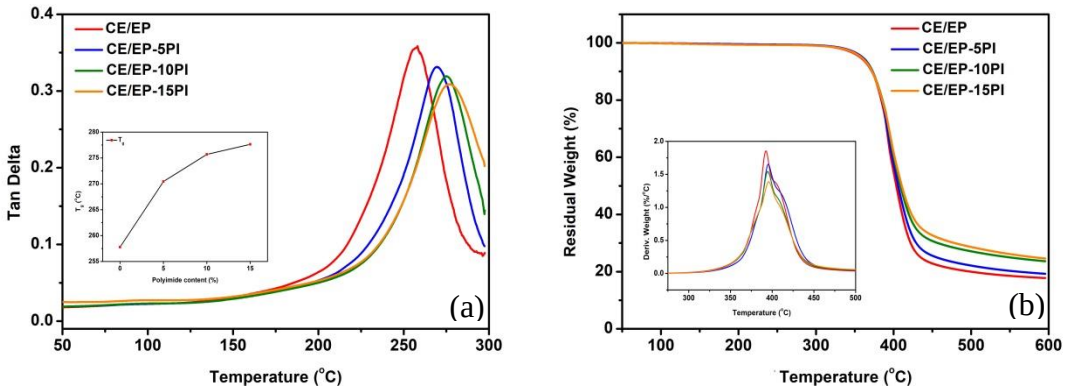

Figure 3.6 – Thermal properties of CE/EP-PI (a) DMA Tan Delta and T_g of CE/EP-PI and (b) TGA scans of degradation behavior of CE/EP-PI

Table 3.3 – Density of CE/EP-PI

	CE/EP	CE/EP-5PI	CE/EP-10PI	CE/EP-15PI
Density (g/cm^3)	1.192 ± 0.006	1.195 ± 0.008	1.200 ± 0.008	1.198 ± 0.005

*test conducted under room temperature

Low Viscosity is essential to ensure the processability of epoxy molding compound since 70-90 % of the fillers will be added into the polymer matrix to control the final compound properties such as CTE and modulus.[10] The viscosity and dielectric properties of CE/EP-PI are shown in Table 3.4. The viscosity of CE/EP-PI was around 0.08 – 0.1 pa·s at 120 ℃, being comparable to that of generally used epoxy resins such as bisphenol A diglycidyl ether (DGEBA) and biphenyl epoxy, which have viscosity ranging from 0.05 pa·s to 5 pa·s depending on the temperature.[90-92] The low viscosity of CE/EP-PI copolymer rendered it high potential to be applied as base resin for molding compounds.

Table 3.4 – Viscosity of CE/EP-PI

Specimen	Viscosity (pa·s)
CE/EP	0.083 ± 0.027
CE/EP-5PI	0.079 ± 0.024
CE/EP-10PI	0.082 ± 0.035
CE/EP-15PI	0.104 ± 0.030

*test conducted at 120 ℃

The dielectric properties greatly affect the reliability of an encapsulation material for high power device. The dielectric permittivity was 2.5 – 2.9 and the loss factor were

around 0.005 – 0.008 from 10 MHz to 1GHz (Table 3.5). The incorporation of polyimide which has a dielectric constant of 3.55 and a loss factor of 0.0034 didn't affect the dielectric properties of CE/EP system much (Table 3.1).

Table 3.5 – Dielectric properties of CE/EP-PI

Specimen	Permittivity			Loss Factor		
	10 MHz	*100 MH*	*1 GHz*	*10 MHz*	*100 MH*	*1 GHz*
CE/EP	2.88	2.85	2.73	0.007	0.005	0.006
CE/EP-5PI	2.78	2.76	2.68	0.007	0.005	0.006
CE/EP-10PI	2.91	2.88	2.80	0.006	0.006	0.008
CE/EP-15PI	2.64	2.62	2.50	0.008	0.005	0.005

* test conducted under room temperature

3.3.3 Effect of High Temperature Aging

3.3.3.1 Modulus and T_g

Long term reliability at high temperature is a prerequisite for epoxy molding compounds subjected to elevated working temperature. Generally, epoxy suffers from a series of thermal aging reactions including bond breaking, thermo-oxidation and chain scission.[93] These reactions can result in the degradation in thermal and mechanical properties, which ultimately leads to material failures. In order to further study the long term effects of high temperature aging on the resin properties, changes in storage

modulus and T_g in DMA measurement were monitored at 200 ℃ over time. The storage modulus during aging tests is shown in Figure 3.7. For CE/EP, the storage modulus increased from 900 MPa to 2,670 MPa after 5-day-aging, and it continued to increase to 3,100 MPa after aging for 10 days (Figure 3.7a). The increase in modulus can be explained by two different steps during aging. In the first step, a post-cure occurred while the crosslinking reactions continued, resulting in an increased modulus. In the second step, the chain scission mechanism was predominant which broke the long chain polymer backbones and rearranged the chain segments into the regions of denser cross linkages.[31-32, 94] This degradation mechanism rendered a stiffened resin with a higher modulus but a lower strain at break and lower fracture toughness. For CE/EP-10PI, the initial storage modulus was more than two times higher than CE/EP, suggesting the formation of a denser structure. In addition, the increase in storage modulus after the high temperature aging was much less than that of CE/EP, indicating that the chain scission effect in resin with polyimide was less significant (Figure 3.7c). The aging storage modulus changes of CE/EP-5PI and CE/EP-15PI were shown in Figure 3.7b and Figure 3.7c. It is interesting to see that CE/EP-15PI had a storage modulus even lower than CE/EP-5PI. Excessive polyimide may aggregate and interrupt the initial formation of CE/EP network as shown in Scheme 3.3. Excess polyimide in this system exhibited low modulus since its continuous network was disturbed.

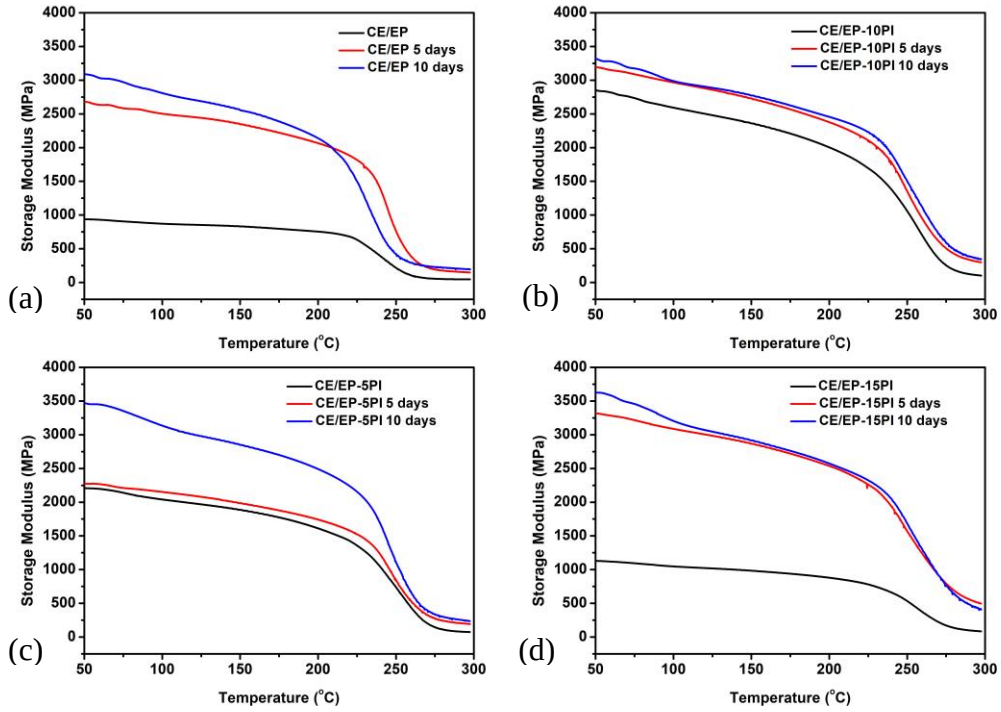

Figure 3.7 – DMA storage modulus of (a) CE/EP (b) CE/EP-5PI (c) CE/EP-10PI (d) CE/EP-15PI in 200 °C aging tests

Figure 3.8 shows the change in T_g of CE/EP-PI during high temperature aging tests. Resins with more polyimide still exhibited a higher T_g after aging, while the trends of resins with different formulae varied. The CE/EP showed an increase in T_g after the first 5 days of aging. In the meanwhile, a slight drop in T_g was observed in CE/EP-5PI, CE/EP-10PI and CE/EP-15PI. It was noted that T_g of CE/EP decreased quickly after 5 days, while resins with polyimide had showed much slower decline of T_g. These results further proved that the incorporation of polyimide can enhance the thermal stability of CE/EP polymer network and help to maintain its mechanical and thermal properties.

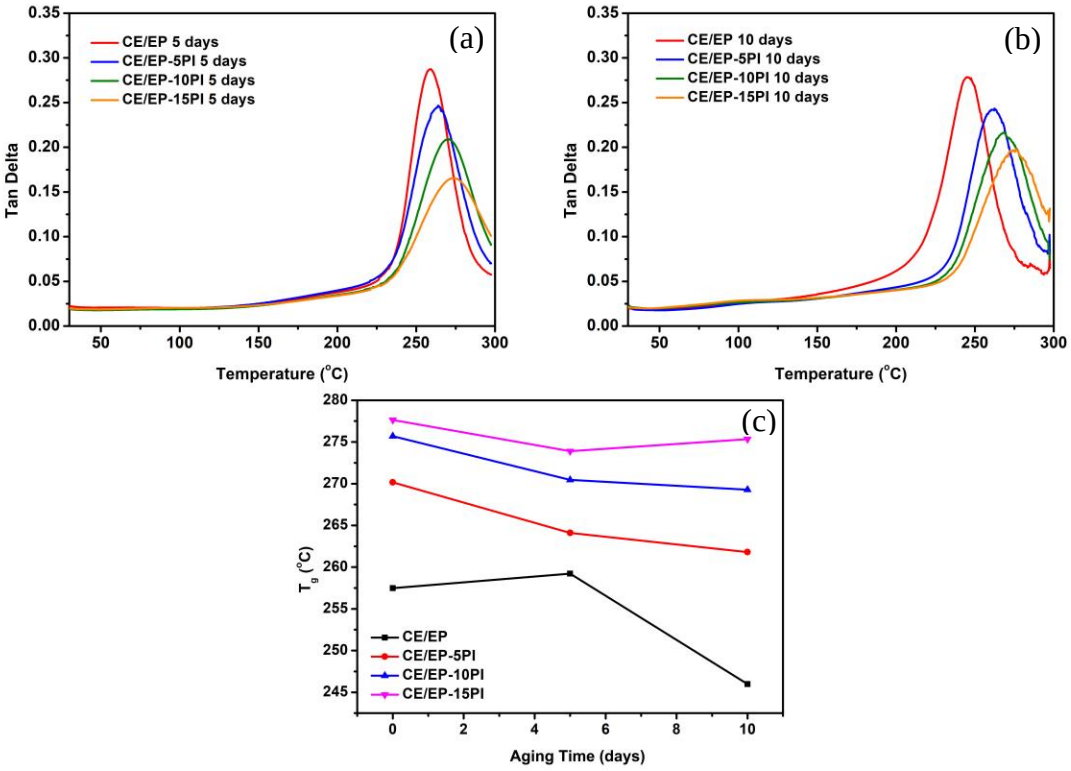

Figure 3.8 – DMA tan delta of CE/EP-PI after (a) 5 days of aging (b) 10 days of aging and (c) T_g changes of CE/EP-PI in 200 ℃ aging tests.

To verify the occurrence of thermo-oxidation reactions, FTIR spectra of CE/EP-PI aged for 48 h was taken (Figure 3.9). The increasing intensity and broadened peak around 3200 cm^{-1} suggested the formation of –OH during hydrolysis, and the broaden peaks around 1700 cm^{-1} was due to the formation of carbonyl groups via thermo-oxidation.[70] Resins with different content of polyimide exhibited similar IR spectra after aging and was similar with that of CE/EP. Therefore, most aging chemical changes occurred in the CE/EP network with the polyimide part left unaffected.

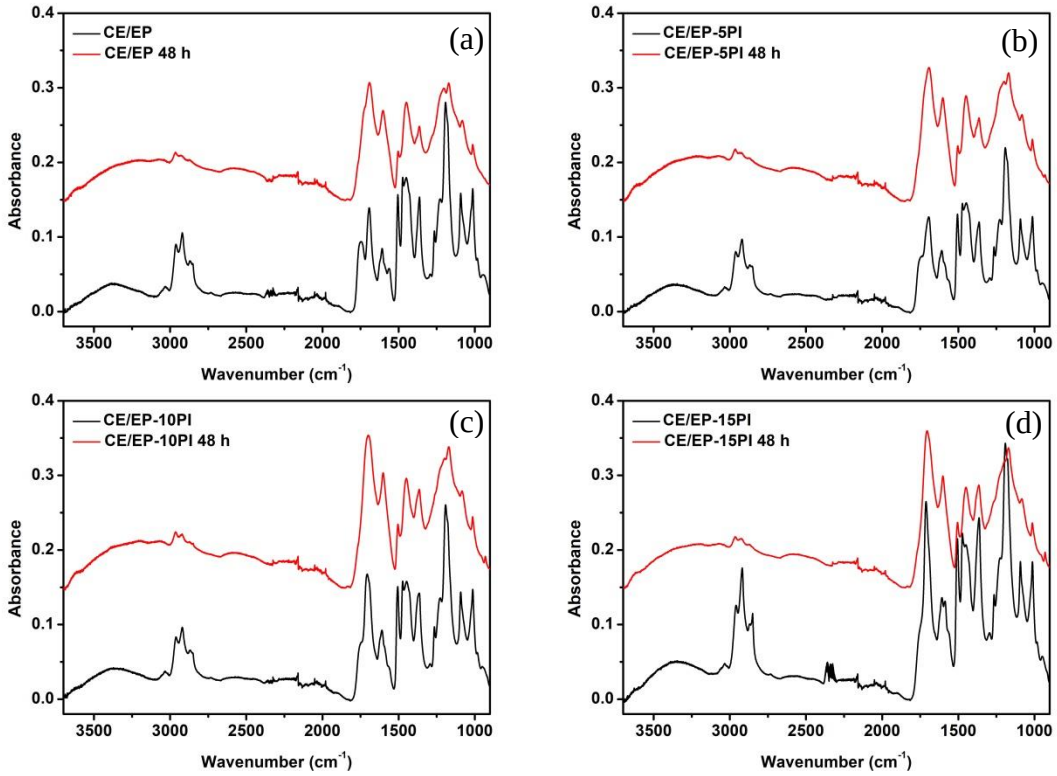

Figure 3.9 – Aging FTIR spectra of (a) CE/EP (b) CE/EP-5PI (c) CE/EP-10PI (d) CE/EP-15PI

3.3.3.2 Fracture Toughness

Epoxy and cyanate ester resins have excellent thermal and mechanical properties, but their high crosslinking density results in the high brittleness and low fracture toughness.[95-96] To make things worse, high temperature aging reactions such as chain scission can even lower down the fracture toughness. In order to study the effect of polyimide incorporation on the resin fracture resistance under high temperature aging, three point bending tests were conducted on samples with different polyimide loading. As shown in Figure 3.10, fracture toughness was suggested by the critical stress intensity factor (K_{IC}), which increased from 1.61 MPa·m$^{1/2}$ to 2.06 MPa·m$^{1/2}$ upon addition of 10% polyimide. The K_{IC} decreased slightly to 1.93 MPa·m$^{1/2}$ when the polyimide loading

further increased to 15%. Incorporation of polyimide at moderate loading (5-10%) into the CE/EP network increased the plastic deformation of the resin, thus leading to higher fracture toughness[95], while too much polyimide resulted in large phase separation and declined physical properties. After aged at 200 ℃ for 10 days, all CE/EP-PI showed increased fracture toughness except for neat CE/EP resin. The drop in fracture toughness of CE/EP after aging may be due to the increased crosslinking density caused by thermo-oxidation. After high temperature aging, polyimide dispersed more evenly in the CE/EP copolymer network, which provided a better fracture toughness. CE/EP-10PI can reach a maximal K_{IC} of 2.55 MPa·$m^{1/2}$ after ten days' aging. The K_{IC} obtained by CE/EP-PI system was a lot higher compared to the values of other epoxy based resin reported in literatures, such as 0.8-1.2 MPa·$m^{1/2}$ for polysulfone modified epoxy,[95] 0.9-1.2 MPa·$m^{1/2}$ for graphene oxide/epoxy composite,[97] and 1.1-1.3 MPa·$m^{1/2}$ for carbon fibre incorporated epoxy.[98]

To further prove the effect of polyimide on fracture toughness, fracture surfaces of CE/EP-PI were observed by SEM (Figure 3.11). CE/EP exhibited a relatively smooth fracture surface with low toughness (Figure 3.11a). In the meanwhile, more fibril structures were formed on the fracture surfaces of CE/EP-PI, indicating the elongation and deformation of resins with enhanced toughness, which may be explained by *in situ* toughness enhancement mechanism (Figure 3.11c, e and g).[99-100] In CE/EP-PI, voids are initiated first between polyimide and epoxy matrix when the resin was subjected to external force since there is no chemical bonding through this interface. The formation of voids then allows larger plastic deformation which can absorb crack energy and thus provide a high toughness. The surface morphologies of resins after aging at 200 ℃ for 10

days were significantly different from their initial morphologies. The fracture surface of CE/EP became much smoother after aging, accounting for a largely increased brittleness (Figure 3.11b). Both CE/EP-10PI and CE/EP-15PI showed dimple-like structures instead of parallel crack structures, which suggested shear deformation (Figure 3.11f and h).[95, 101] The fracture surface morphology further confirmed that the incorporation of polyimide greatly increased the fracture toughness of CE/EP resin and performed even better under high temperature.

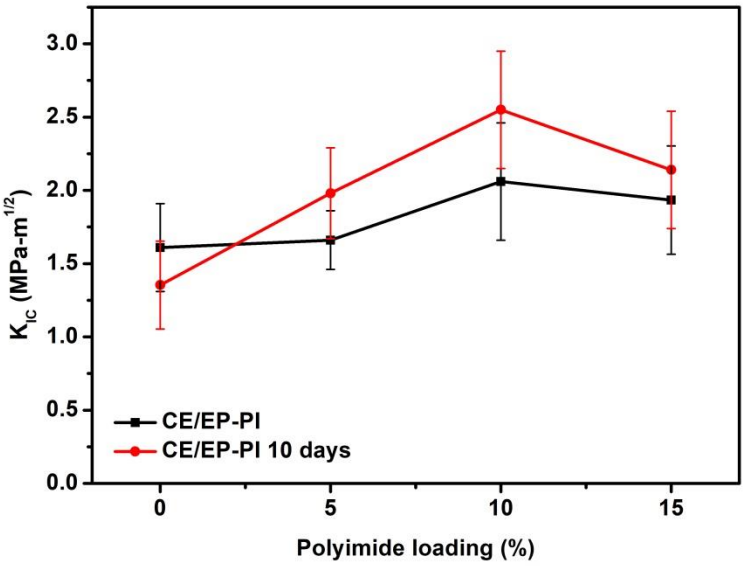

Figure 3.10 – K_{IC} of CE/EP-PI and CE/EP-PI aged at 200 °C

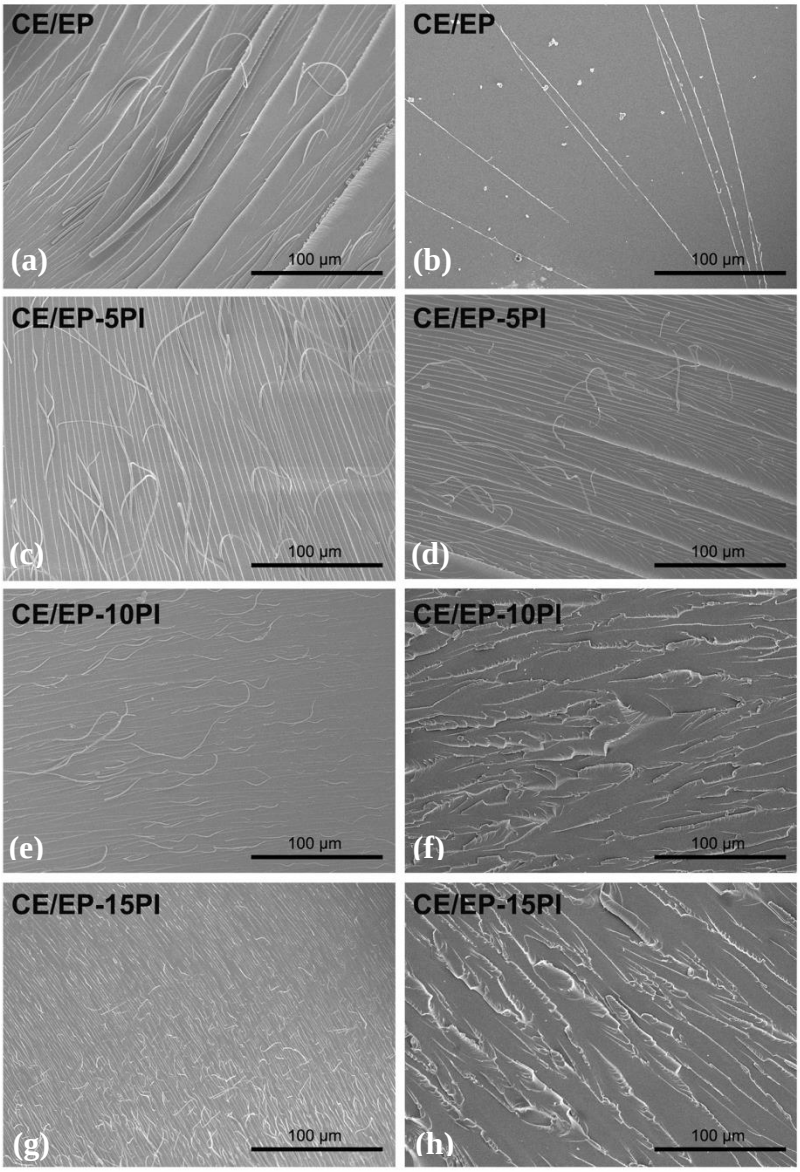

Figure 3.11 – SEM images of (a) CE/EP (b) CE/EP aged for 10 days (c) CE/EP-5PI (d) CE/EP-5PI aged for 10 days (e) CE/EP-10PI (f) CE/EP-10PI aged for 10 days (g) CE/EP-15PI and (h) CE/EP-15PI aged for 10 days

3.3.4 Thermal Stability and Moisture Absorption

Mass loss of the resin upon thermal aging was investigated at 200 ℃, as shown in Figure 3.12. During the high temperature aging, volatile products released from the polymer network and resulted in a mass loss of the resins.[102] The degradation of CE/EP

polymer network involves the hydrolysis reaction of polycyanurate, which breaks the triazine network and produces small molecules of CO_2 and NH_3.[58, 70] In the CE/EP-PI system, the incorporation of polyimide reduced the overall mass loss of the resins since polyimide itself had an excellent thermal stability. As expected, CE/EP-15PI had the least mass loss during the high temperature aging test. The slight increase in the resin mass observed before 100 h might correspond to the oxidation of resin.[32, 103]

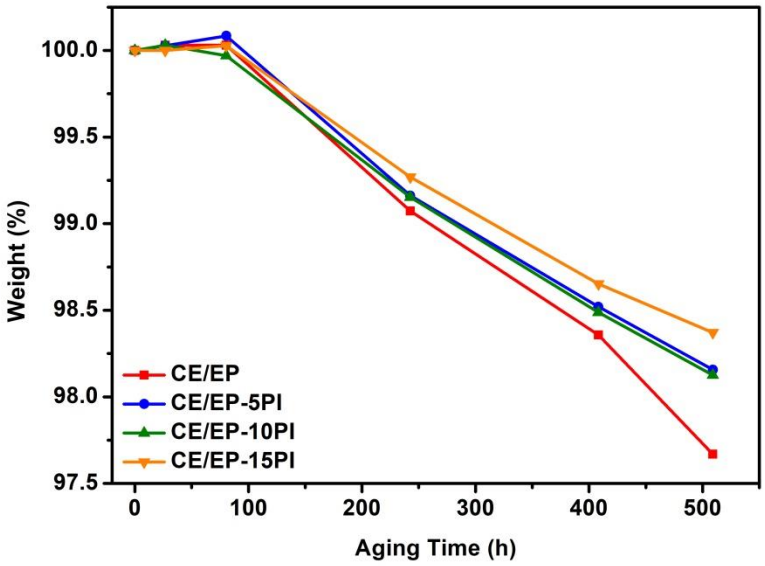

Figure 3.12 – 200 ℃ aging mass loss of CE/EP-PI

Moisture absorption rate was another important factor to evaluate the long-term stability of the CE/EP-PI system. As shown in Figure 3.13, the equilibrium moisture absorption rate increased with the addition of polyimide in the resin. CE/EP-15PI showed moisture absorption of 1.7% at equilibrium in boiling water, larger than the value of 1.3% for CE/EP. Polyimide generally has a high affinity for water with an equilibrium water uptake up to 6% due to its polar structure, which may cause plasticization, hydrolysis and swelling of the resin.[104-105] Therefore, the trade-off between thermal stability and

moisture adsorption requires further research effort for the optimization of the copolymer blends system.

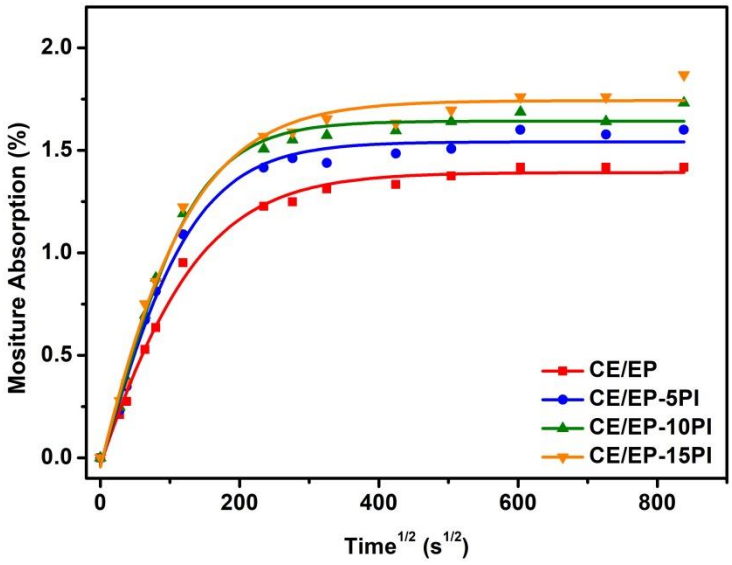

Figure 3.13 – Moisture absorption of CE/EP-PI

3.4 Conclusion

In this chapter, polyimide modified CE/EP polymers with excellent thermal stability and long term reliability were prepared. Aromatic polyimide has good dispersity in CE/EP copolymer for their similarity in aromatic structures. The denser network structure formed via polyimide incorporation provided increased T_g, modulus and fracture toughness. The T_g increased by 13 ℃ with only 5% of polyimide, and a maximum T_g of 278 ℃ was achieved for CE/EP-15PI. In addition, it was observed that polyimide aggregation can lead to phase separation at high polyimide loadings. In the high temperature aging tests, CE/EP-PI demonstrated better retention of its thermal and mechanical properties than CE/EP, with no deterioration in T_g, less increase in modulus, higher thermal stability and fracture toughness. The maximal fracture toughness of

CE/EP-10PI was as high as 2.55 $MPa \cdot m^{1/2}$ after aging, which were among the top compared with other reported values in literature. It was also found that the addition of polyimide increased the moisture absorption of the resin. To sum up, the optimized polyimide amount is to be determined around 5%-10%, which can offer significant improvement in T_g, thermal stability, fracture toughness and high temperature aging performance. The CE/EP-PI system in this study exhibited promising properties for application in high temperature molding compounds.

CHAPTER 4. RUBBERIZED SILICON CARBIDE PARTICLES FOR THERMAL CONDUCTIVITY IMPROVEMENT

4.1 Background

With the rapid development of high power, high frequency and high density electronics, heat management of the package has attracted intensive attention. Thermal conductivity is becoming an increasingly important parameter in the evaluation of packaging materials like EMCs. However, for polymer encapsulation materials such as epoxy, their low thermal conductivity by nature due to the phonon scattering issue greatly limits their ability of heat dissipation. Therefore, it is worthwhile to look into the modification of filler system for the improvement of thermal conductivity in EMCs as an alternative.

Filler composes 70-90% of the EMC and largely determines the CTE, modulus, toughness and thermal conductivity of the compound. Generally, silica fillers are used in EMC for its low CTE, but the thermal conductivity of silica is only ~1.3 W/mK, which is quite low compared to some other ceramic fillers like SiC and BN.[106] By replacing silica with high thermally conductive fillers, the thermal conductivity of the polymer composites can be increased as theoretically predicted by different models such as Maxwell-Garnett model and Bruggeman model.[22] Experimentally, Al_2O_3 was reported to increase the thermal conductivity of epoxy to 4.3 W/mK with a volume fraction of 60% by Kozako *et al.*[107] Lee and his group developed a hybrid filler system based on AlN and SiC (60 vol.%) and obtained HDPE composites with thermal conductivity of 2.25

W/mK.[108] Despite the various studies and development on filler system for high thermal conductivity polymer composites, effects of surface treatment of fillers on compound properties haven't been well studied yet.

In this work, SiC particles are treated with silane and reactive silicone respectively. SiC with different coating layers were loaded into epoxy matrix and formed epoxy composites. The effects of different SiC fillers on thermal conductivity and toughness of the epoxy composites were investigated. This study promotes the understanding of filler-matrix interface in EMCs.

4.2 Experimental Section

4.2.1 Materials

(3-Glycidoxypropyl)trimethoxysilane (GPTMS) and aminopropyl terminated polydimethylsiloxane with molecular weight of 3000 (DMS-A15) were purchased from Gelest, Inc. Formic acid was obtained from Fisher Scientific. Tetra methyl biphenyl epoxy with an epoxide equivalent weight of 197 was purchased from Mitsubishi Chemical Corporation. Aluminum acetylacetonate catalyst was purchased from Aldrich Chemical Company, Inc. Curing agent, hexahydro-4-methylphthalic anhydride (HMPA), was purchased from Lindau Chemicals, Inc. The chemical structures of the major chemicals used are shown in Scheme 4.1

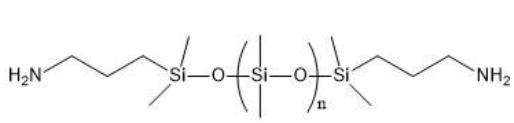

Aminopropyl Terminated Polydimethylsiloxane

(a)

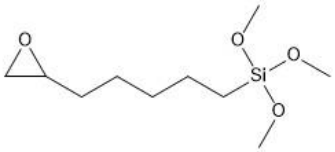

(3-Glycidoxypropyl)trimethoxysilane

(b)

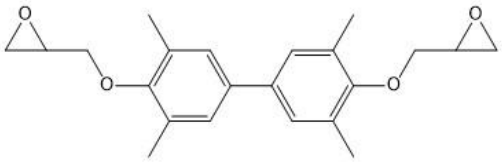

Tetra methyl biphenyl epoxy

(c)

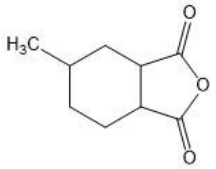

Hexahydro-4-methylphthalic anhydride

(d)

Scheme 4.1 – Chemical structures of (a) aminopropyl terminated polydimethylsiloxane (b) (3-glycidoxypropyl)trimethoxysilane (c) tetra methyl biphenyl epoxy (d) hexahydro-4-methylphthalic anhydride

4.2.2 Preparation of rubberized SiC and Filled Epoxy Compounds

The surface functionalization of SiC by silanes was conducted according to the method reported by Liang *et al.*[109] SiC particles were first oxidized at 1200 ℃ for 3 h in oven. 1 g of surface oxidized SiC (SiC-SiO_2) was dispersed in ethanol and sonicated for 30 min. Then 1 g of water and 0.2 ml of GPTMS was added into the solution and the pH was tuned to 4 by formic acid. The solution was refluxed at 80 ℃ for 24 h to ensure the grafting of the silane on SiC particles. The silane coated SiC-SiO_2 particles (SiC-GPTMS) were filtered and dried at 120 ℃ for 6 h. To coat a rubberized layer outside the particles, 1 g of SiC-GPTMS and 0.5 ml of DMS-A15 were mixed in ethanol, refluxed for 24 h, filtered and dried. SiC coated by DMS-A15 is designated as SiC-A15. Scheme 4.2 shows the preparation steps of surface treated SiC.

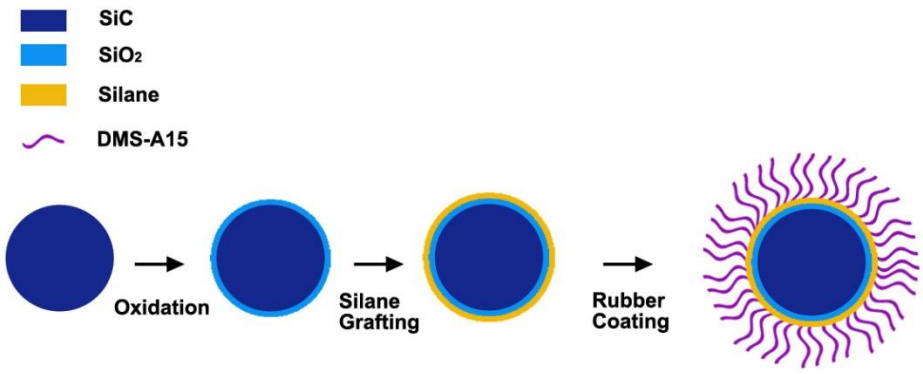

Scheme 4.2 – Schematic representation of sample preparation

In the preparation of epoxy compounds, tetra methyl biphenyl epoxy and hexahydro-4-methylphthalic anhydride were mixed at a ratio of 1:0.85. The mixture was melt and stirred continuously at 100 ℃ until a homogeneous phase was obtained. Different fillers were loaded into the epoxy melts as shown in Table 4.1. Filled epoxy samples were cured at 210 ℃ for 2 h with 0.3% of catalyst.

Table 4.1 – Epoxy compound formulas with different filler loadings

Specimen	Epoxy and hardener (%)	SiC-GPTMS (%)	SiC-A15 (%)
Ep	100	-	-
Ep-10SiC-GPTMS	90	10	-
Ep-30SiC-GPTMS	70	30	-
Ep-10SiC-A15	90	-	10

Table 4.1 continued

Ep-30SiC-A15	70	-	30

4.2.3 Characterization of rubberized SiC and Filled Epoxy Compounds

An XPert PRO Alpha-1 XRD was performed to study the crystal structure of the pristine SiC powder and the surface oxidized SiC. The coated SiC was chemically characterized by Thermo Scientific iS50 FT-IR Spectrometer to investigate the chemical structures. A TGA Q50 from TA Instruments was used to obtain the amount of the rubber coated. In order to study the thermal conductivity of the epoxy compounds, a LFA 467 HyperFlash from Netzsch was performed to obtain the thermal diffusivity of the compounds. The heat capacity and density needed in the calculation of thermal conductivity were achieved respectively by DSC Q2000 from TA Instruments and density measurement based on Archimedes' principle. Thermal conductivity was obtained based on the following equation.

$$\kappa = \alpha \times \rho \times C_p \quad (4)$$

Where κ is the thermal conductivity (W/mK), α is the thermal diffusivity (m^2/s), ρ is the density (kg/m^3) and C_p is the heat capacity (J/(kg·K)). In the measurement of fracture toughness of the compounds, three point bending tests were conducted by Instron 5548 MicroTester according to ASTM E-399. The morphology of both fillers and fracture surfaces of the compounds were observed by Hitachi SU8010 SEM.

4.3 Results and Discussion

4.3.1 Surface Treatment of SiC

In the surface treatment of SiC, it is necessary to form an oxidation layer and thus enhance the reactivity of the particles, since the SiO_2 oxidation layer provides more silanol groups than SiC. XRD scans of SiC and SiC-SiO_2 are shown in Figure 4.1. SiC powder exhibited peaks at 34.04 º, 34.70 º, 35.57 º, 38.08 º, 59.95 º, 65.55 º and 71.70 º, which confirmed its hexagonal crystal structure.[110-111] SiC-SiO_2 showed an extra peak at 21.78 º, which was corresponding to the (011) planes of hexagonal SiO_2.[112]

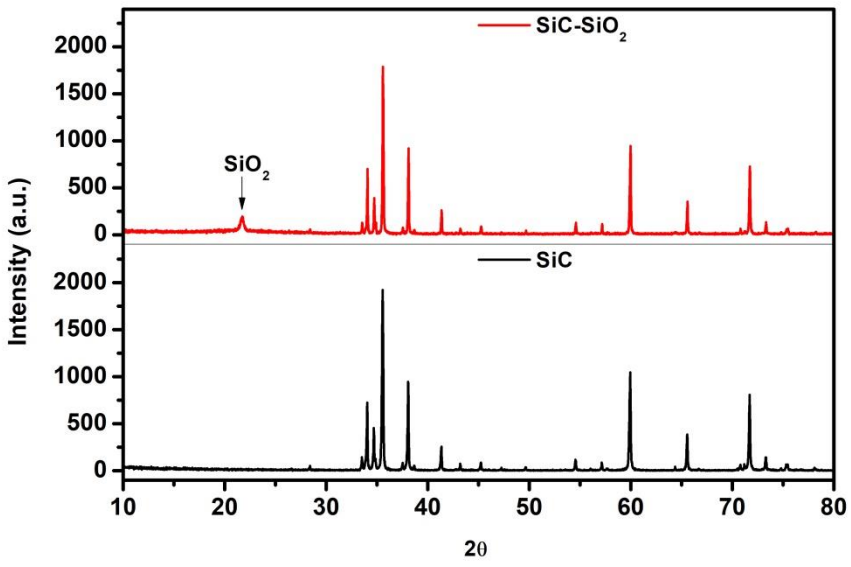

Figure 4.1 – XRD scan of SiC and SiC-SiO2 particles

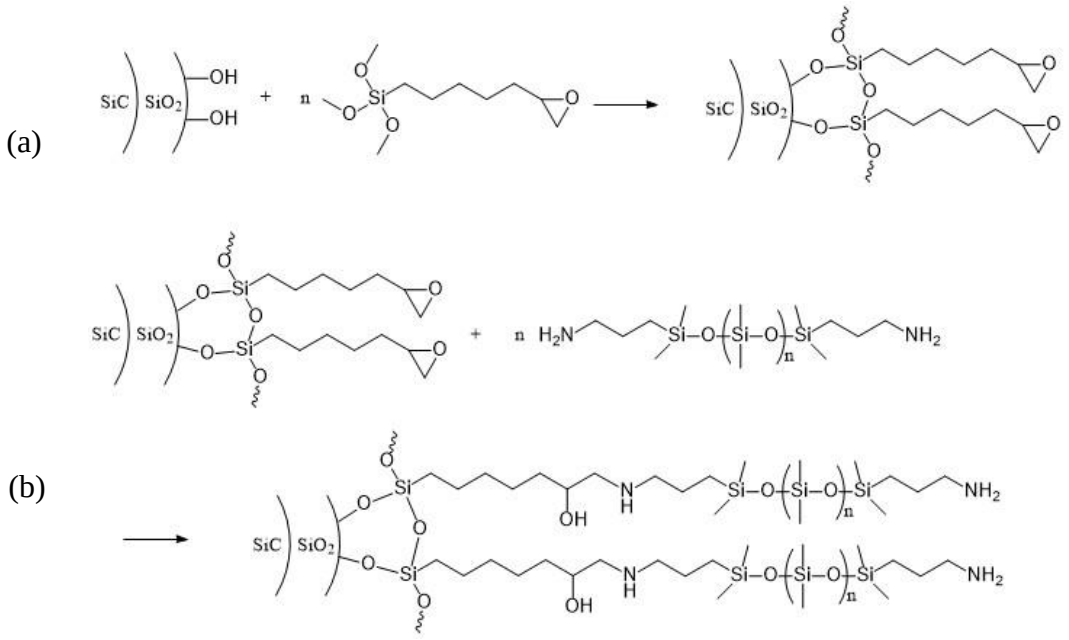

Scheme 4.3 – Chemical reactions of (a) GPTMS grafting (b) DMA-15 coating

With more reactive sites provided by SiO_2 oxidation layer, GPTMS and DMS-A15 were grafted to the particle surface (Scheme 4.3). GPTMS attached to the silica surface via a hydrolysis reaction, and its epoxide terminated group further reacted with the anime terminated group of DMS-A15, which ensured the rubber layer coating. Chemical structures of the double layer coating were investigated and confirmed by FTIR (Figure 4.2). For both SiC-GPTMS and SiC-A15, the strong peak at 1000-1200 cm^{-1} was corresponding to the Si-O-Si bonding. The peak at 2990 cm^{-1} of SiC-GPTMS can be attributed to –OH groups, while the peak at 2960 cm^{-1} of SiC-A15 can be attributed to N-H stretching. The sharp peak at 1256 cm-1 represents the C-N stretching of primary amine, confirming the coating of DMS-A15 in SiC-A15.[113] The amount of the coating layer grafted to the SiC surface was investigated by TGA. SiC-GPTMS exhibited a mass loss of 0.06 % when heated from 120 ℃ to 450 ℃, which indicated the amount of silane

grafting layer. Compared to SiC-GPTMS, SiC-A15 had a larger mass loss of 0.23 %. Therefore, the weight corresponding to the rubber layer was around 0.17 %.

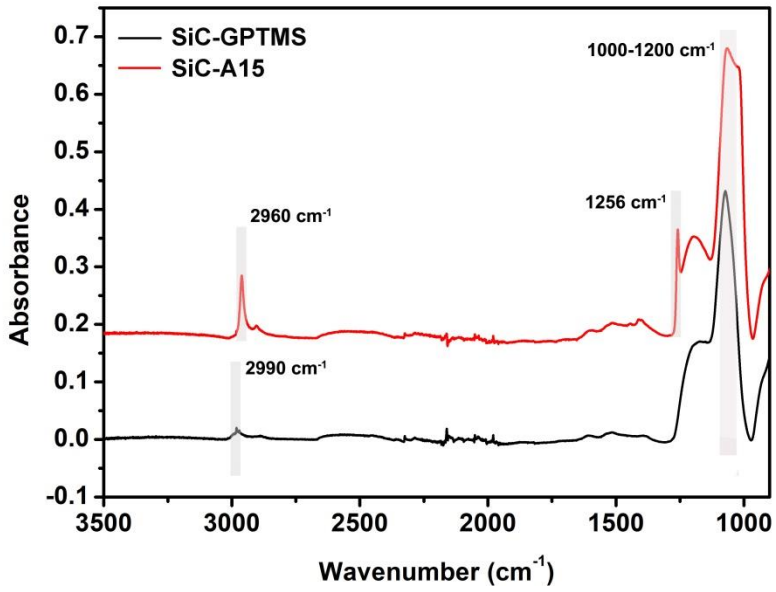

Figure 4.2 – FTIR spectra of treated SiC

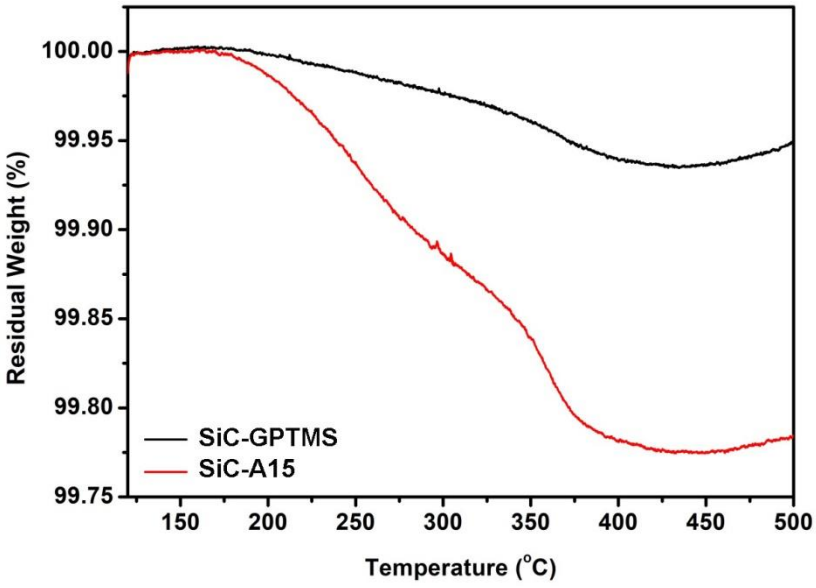

Figure 4.3 – TGA scans of modified SiC

4.3.2 Properties of Epoxy Compoistes

The effect of treated SiC filler on the thermal conductivity of the compounds is shown in Figure 4.4. The thermal conductivity increased gradually with the filler loading. The thermal conductivity of Ep-30SiC-A15 reached 0.29 W/mK, which was about three times of the neat epoxy. The thermal conductivity is expected to increase further with more filler loading, when more contacts between fillers are formed and construct good paths for heat transfer.[114] Compared with SiC-GPTMS, SiC-A15 offered a larger increase in compound thermal conductivity. To study the difference between SiC-GPTMS and SiC-A15 in epoxy matrix, SEM images of the composite fracture surfaces were taken (Figure 4.5). As shown in Figure 4.5a, the irregular polyhedral SiC particle had a size of 3-5 μm. SiC-GPTMS exhibited good dispersion in epoxy matrix, while Ep-30SiC-A15 showed filler aggregation caused by interaction between rubber layers. This aggregation of fillers created more contacts between these polyhedral particles and more thermally conductive paths. Therefore, epoxy with SiC-A15 had a higher thermal conductivity than epoxy with SiC-GPTMS at the same filler loading level.

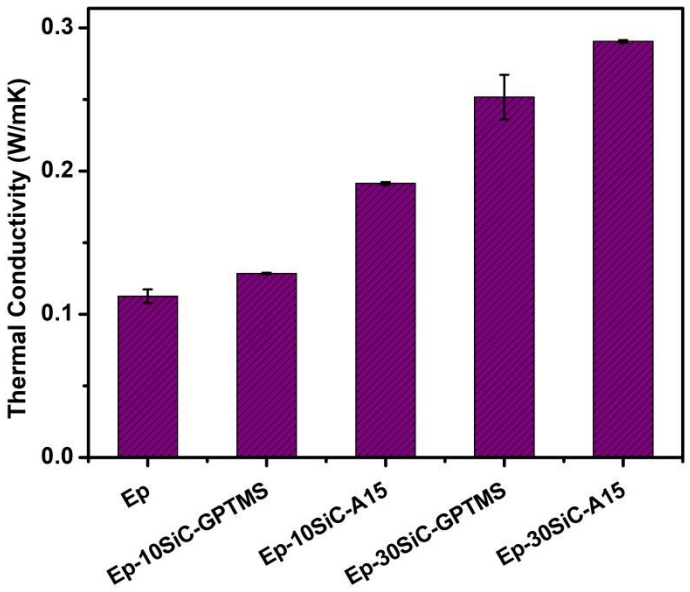

Figure 4.4 – Thermal conductivity of epoxy compounds with modified fillers

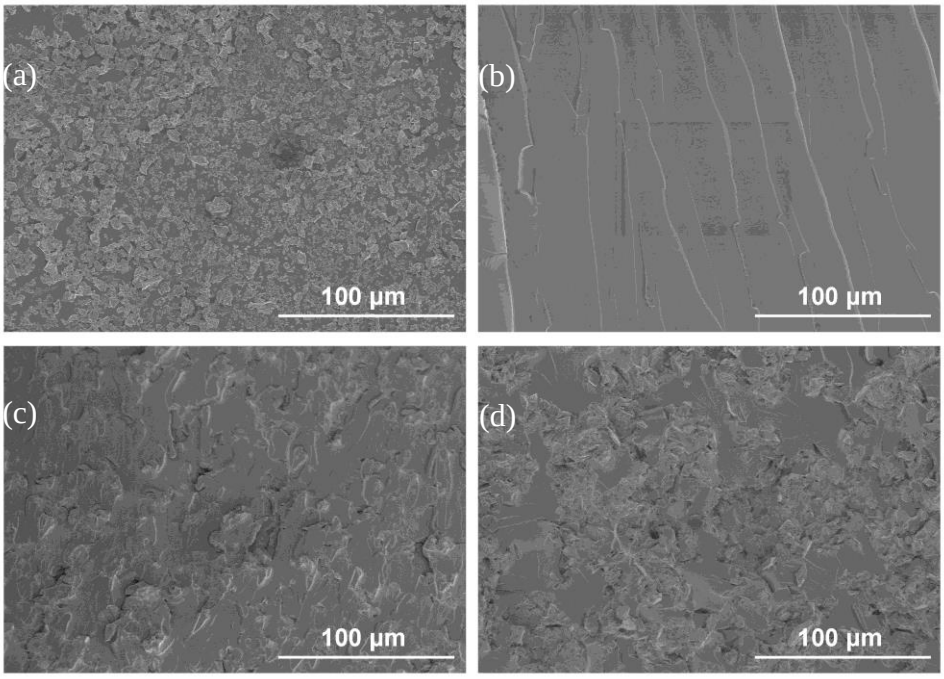

Figure 4.5 – SEM images of (a) SiC particles (b) fracture surface of epoxy resin (c) fracture surface of Ep-30SiC-GPTMS (d) fracture surface of Ep-30SiC-A15

Fracture toughness is also an important property affected by filler in EMC. Generally, fracture toughness decreases with filler loading because of the weak interface between filler and matrix where cracks tend to propagate.[115] The fracture toughness of epoxy with different fillers was indicated by K_{IC} shown in Figure 4.6. K_{IC} decreased from 3 Mpa·$m^{1/2}$ to 1.5 Mpa·$m^{1/2}$ with 30% of filler. There was no significant difference between SiC-GPTMS and SiC-A15. However, SEM images of the fracture surface showed different failure mechanisms for SiC-GPTMS and SiC-A15. Although Ep-30SiC-GPTMS had a better dispersion of filler, the cracks propagated along the filler-matrix interface, leaving a relatively smooth fracture surface (Figure 4.5c). In Ep-30SiC-A15 the crack broke through the aggregation regions of the rubberized fillers instead of the filler-matrix interface (Figure 4.5d). The rubber layer formed by amine terminated silicone provided a better interface between filler and epoxy since the amine groups can react with epoxy matrix and form covalent bonding. Figure 4.5b is the fracture surface of neat epoxy for reference.

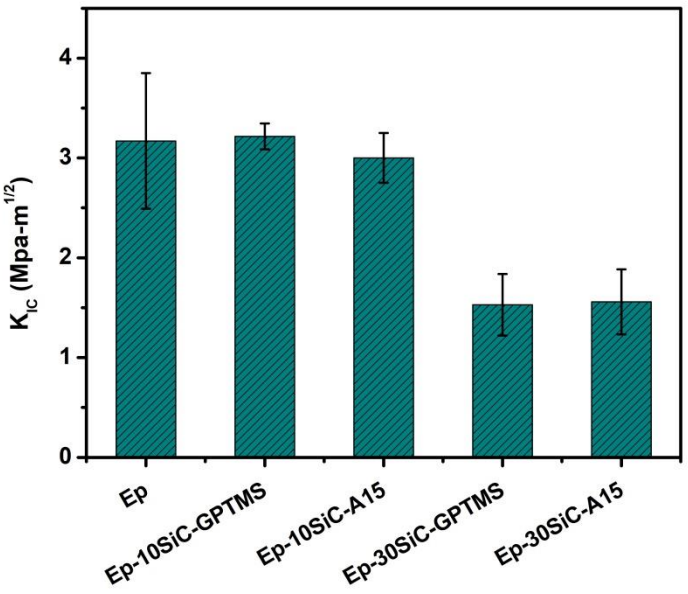

Figure 4.6 – Fracture toughness of epoxy compounds with modified fillers

4.4 Conclusion

In this chapter, SiC particles were coated with silane and silicone rubber layer. SiC treated with silane had a better dispersity in epoxy matrix while SiC with silicone rubber layer tended to aggregate with each other and formed separated filler regions. Despite different filler morphology in composites, both treated fillers increased the thermal conductivity of the epoxy composites. Epoxy with 30% of SiC-A15 had a thermal conductivity of 0.29 W/mK. On the other hand, fracture toughness decreased a lot after filler loading. Epoxy with SiC-GPTMS and SiC-A15 showed different failure mechanism in crack propagation. For SiC-GPTMS, the filler-matrix interface was the weak point. For SiC-A15, reactive rubber layer provided strengthened interface. Therefore, crack broke though the filler aggregations instead of the interface.

CHAPTER 5. FUTURE WORK

5.1 Control of Coating Thickness in SiC Surface Treatment

In Chapter 4, we fabricated surface treated SiC fillers and successfully increased the thermal conductivity of the polymer composites. The coating amount was characterized by high temperature weight loss in TGA tests. The thickness of the surface coating layer may have a large influence on the mechanical properties of EMC, such as CTE, modulus and fracture toughness. In order to have a good control of the coating layer thickness, we can use aminopropyl terminated polydimethylsiloxane with different chain length as shown in Figure 5.1. Compared to DMS-A15 used in Chapter 4, DMS-A11 has a much lower molecular weight of 850-900, which would form a thinner coating layer outside the particles. We have proven that SiC-A15 suffered from aggregation when mixed in the polymer matrix due to the extensive interaction between rubber layers. By fabricate fillers with thinner rubber layer, better dispersity of the filler may be achieved.

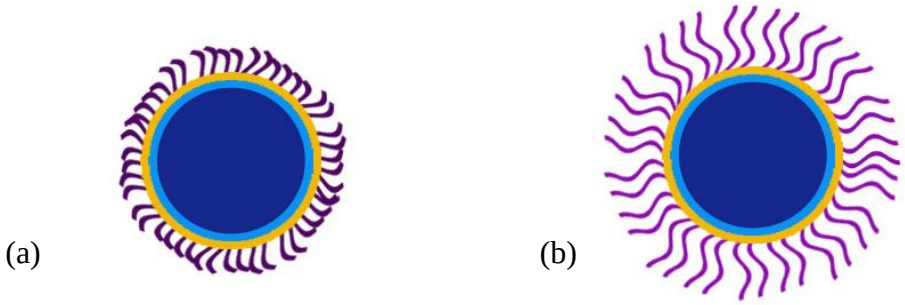

Figure 5.1 – Fillers coated with different aminopropyl terminated polydimethylsiloxane (a) SiC-A11 (b) SiC-A15

Due to the polyhedral shape of the filler particles, the coating thickness cannot be simply calculated based on the weight. Analytical tools such as TEM may be applied in the future study to better characterize the morphology and thickness of the coating layer.

5.2 Application of modified EMC system

In Chapter 2 and 3, polyimde incorporated cyanate ester/epoxy co-curing polymer system was investigated and optimized for high temperature stability. In Chapter 4, modified filler based on surface treated SiC was study to enhance the thermal conductivity of the composites. However, in order to evaluate the potential application of this composite system as an encapsulation material, there are several other properties that need to be considered, such as CTE and viscosity.

The thermo-mechanical stress caused by CTE mismatch is one of the major issues causing package failure in electronic devices. Generally, polymer materials have high CTE due to the lack of strong bonding between polymer chains. The CTEs of CE/EP resins are listed in Table 5.1. The CTEs before T_g are more than 50 ppm. Silica filler with a low CTE of ~1.3 ppm is added into the composite to lower the final CTE of the final compound to 15-20 ppm, in order to reduce the thermo-mechanical stress in a package.[116-117] However, high thermal conductivity fillers such as Al_2O_3 and SiC usually have higher CTE than silica.[118-120] When silica is replaced with these high thermal conductivity fillers, more fillers are needed in the composites to achieve the designated CTE.

Table 5.1 – CTE of CE/EP resins

	CTE before T_g (ppm)	CTE after T_g (ppm)

Table 5.1 continued

Ep	80	161
CE/EP-12	58	248
CE/EP-11	60	200
CE/EP-21	55	180
CE/EP-31	64	109

In chapter 4, SiC with a polyhedral shape were used, which is beneficial for high thermal conductivity because of its high aspect ratio.[22] However, fillers with high aspect ratio result in high viscosity, which is undesirable from processability aspect. Therefore, both CTE and viscosity of the composites need to be taken into consideration in the further study and optimization of this EMC system.

APPENDIX A. AUTHOR'S PUBLICATIONS

A.1 Journal Publications

1. Wu, F.; Tuan, C. C.; Song, B.; Moon, K. S.; Wong, C. P., Controlled synthesis and evaluation of cyanate ester/epoxy copolymer system for high temperature molding compounds. *Journal of Polymer Science Part A: Polymer Chemistry* **2018,** *56* (13), 1337-1345.

2. Song, B.; Wu, F.; Zhu, Y.; Hou, Z.; Moon, K.-S.; Wong, C.-P., Effect of polymer binders on graphene-based free-standing electrodes for supercapacitors. *Electrochimica Acta* **2018,** *267*, 213-221.

3. Chen, Y.; Zhang, C.; Li, L.; Tuan, C.-C.; Wu, F.; Chen, X.; Gao, J.; Ding, Y.; Wong, C.-P., Fabricating and controlling silicon zigzag nanowires by diffusion-controlled metal-assisted chemical etching method. *Nano letters* **2017,** *17* (7), 4304-4310.

4. Yang, W.; Zhang, B.; Zhang, Q.; Wang, L.; Song, B.; Wu, F.; Wong, C., Different valence Sn doping–A simple way to detect oxygen concentration variation of ZnO quantum dots synthesized under ultrasonic irradiation. *Ultrasonics sonochemistry* **2017,** *38*, 29-37.

5. Yang, Z.; Wu, F.; He, Y.; Zhang, Q.; Zhang, Y.; Zhou, G.; Yang, H.; Zhou, P., A novel PTP1B inhibitor extracted from Ganoderma lucidum ameliorates insulin resistance by regulating IRS1-GLUT4 cascades in the insulin signaling pathway. *Food & function* **2018,** *9* (1), 397-406.

6. Yang, Z.; Wu, F.; Yang, H.; Zhou, P., Endocytosis mechanism of a novel proteoglycan, extracted from Ganoderma lucidum, in HepG2 cells. *RSC Advances* **2017,** *7* (66), 41779-41786.

A.2 Conference Proceedings

1. Wu, F.; Song, B., Moon, K.-S.; Wong, C.-P. In *Cyanate ester/epoxy co-curing system with thermal stabilizers for high temperature stability*, Electronic Components and Technology Conference (ECTC), 2018 IEEE 68th, IEEE: 2018; In print.

2. Tuan, C.-C.; Wu, F.; Moon, K.-S.; Wong, C.-P. In *Epoxy/cyanate ester copolymer material for molding compounds in high-temperature operations*, Electronic Components and Technology Conference (ECTC), 2017 IEEE 67th, IEEE: 2017; pp 1328-1333.

REFERENCES

1. Kinjo, N.; Ogata, M.; Nishi, K.; Kaneda, A.; Dušek, K., Epoxy molding compounds as encapsulation materials for microelectronic devices. In *Speciality Polymers/Polymer Physics*, Springer: 1989; pp 1-48.

2. Gan, C.; Classe, F.; Chan, B.; Hashim, U., Effects of bonding wires and epoxy molding compound on gold and copper ball bonds intermetallic growth kinetics in electronic packaging. *Journal of electronic materials* **2014,** *43* (4), 1017-1025.

3. Yao, Y.; Lu, G.-Q.; Boroyevich, D.; Ngo, K. D., Survey of high-temperature polymeric encapsulants for power electronics packaging. *IEEE Transactions on Components, Packaging and Manufacturing Technology* **2015,** *5* (2), 168-181.

4. Zheng, H.; Li, L.; Lei, X.; Yu, X.; Liu, S.; Luo, X., Optical performance enhancement for chip-on-board packaging LEDs by adding TiO 2/silicone encapsulation layer. *IEEE electron device letters* **2014,** *35* (10), 1046-1048.

5. Li, X.; Feng, Y.; Tan, X.; Han, Y.; Sun, X., Performance of methylphenyl hydrogen-containing silicone oils for LED encapsulation. *Journal of Macromolecular Science, Part A* **2017,** *54* (10), 690-694.

6. Lee, G.; Kim, H.; Baek, S.; Choi, H.; Chung, K.; Cho, B.; Lee, S.; Lee, Y.-S., Enhancing the elevated temperature performance of high voltage LiNi0. 5Mn1. 5O4 by V doping with in-situ carbon and polyimide encapsulation. *Journal of Power Sources* **2015,** *298*, 379-384.

7. Nam, J.; Lee, Y.; Choi, W.; Kim, C. S.; Kim, H.; Kim, J.; Kim, D. H.; Jo, S., Transfer Printed Flexible and Stretchable Thin Film Solar Cells Using a Water‐Soluble Sacrificial Layer. *Advanced Energy Materials* **2016,** *6* (21).

8. Wang, X.; Li, G.; Li, J.; Zhang, Y.; Wook, A.; Yu, A.; Chen, Z., Structural and chemical synergistic encapsulation of polysulfides enables ultralong-life lithium–sulfur batteries. *Energy & Environmental Science* **2016,** *9* (8), 2533-2538.

9. Gao, W.; Bie, M.; Liu, F.; Chang, P.; Quan, Y., Self-Healable and Reprocessable Polysulfide Sealants Prepared from Liquid Polysulfide Oligomer and Epoxy Resin. *ACS applied materials & interfaces* **2017,** *9* (18), 15798-15808.

10. Lu, D.; Wong, C., *Materials for advanced packaging*. Springer: 2016.

11. Yeon, S.; Park, J.; Lee, H.-J., Compensation Method for Die Shift Caused by Flow Drag Force in Wafer-Level Molding Process. *Micromachines* **2016,** *7* (6), 95.

12. Wong, C., *Polymers for electronic & photonic application*. Academic Press: San Diego, 1993.

13. Wang, X.; Xing, W.; Feng, X.; Yu, B.; Song, L.; Hu, Y., Functionalization of graphene with grafted polyphosphamide for flame retardant epoxy composites: synthesis, flammability and mechanism. *Polymer Chemistry* **2014,** *5* (4), 1145-1154.

14. Domun, N.; Hadavinia, H.; Zhang, T.; Sainsbury, T.; Liaghat, G.; Vahid, S., Improving the fracture toughness and the strength of epoxy using nanomaterials–a review of the current status. *Nanoscale* **2015,** *7* (23), 10294-10329.

15. Gu, J.; Zhang, Q.; Dang, J.; Xie, C., Thermal conductivity epoxy resin composites filled with boron nitride. *Polymers for Advanced Technologies* **2012,** *23* (6), 1025-1028.

16. Jones, E. A.; Wang, F. F.; Costinett, D., Review of commercial GaN power devices and GaN-based converter design challenges. *IEEE Journal of Emerging and Selected Topics in Power Electronics* **2016,** *4* (3), 707-719.

17. Shenai, K.; Dudley, M.; Davis, R. F., Current status and emerging trends in wide bandgap (WBG) semiconductor power switching devices. *ECS Journal of Solid State Science and Technology* **2013,** *2* (8), N3055-N3063.

18. Sheng, K., Maximum junction temperatures of SiC power devices. *IEEE Transactions on Electron Devices* **2009,** *56* (2), 337-342.

19. Liu, Y.; Kinzer, D. In *Challenges of power electronic packaging and modeling*, Thermal, Mechanical and Multi-Physics Simulation and Experiments in Microelectronics and Microsystems (EuroSimE), 2011 12th International Conference on, IEEE: 2011; pp 1/9-9/9.

20. Odegard, G.; Bandyopadhyay, A., Physical aging of epoxy polymers and their composites. *Journal of Polymer Science Part B: Polymer Physics* **2011,** *49* (24), 1695-1716.

21. De Vreugd, J.; Jansen, K.; Ernst, L.; Bohm, C.; Pufall, R. In *High temperature storage influence on molding compound properties*, Thermal, Mechanical & Multi-Physics Simulation, and Experiments in Microelectronics and Microsystems (EuroSimE), 2010 11th International Conference on, IEEE: 2010; pp 1-6.

22. Chen, H.; Ginzburg, V. V.; Yang, J.; Yang, Y.; Liu, W.; Huang, Y.; Du, L.; Chen, B., Thermal conductivity of polymer-based composites: Fundamentals and applications. *Progress in Polymer Science* **2016,** *59*, 41-85.

23. Akatsuka, M.; Takazawa, Y.; Sugawara, K., Thermosetting resin compounds. Google Patents: 2006.

24. Zhou, Y.; Bai, Y.; Yu, K.; Kang, Y.; Wang, H., Excellent thermal conductivity and dielectric properties of polyimide composites filled with silica coated self-passivated aluminum fibers and nanoparticles. *Applied Physics Letters* **2013,** *102* (25), 252903.

25. Giannazzo, F.; Fisichella, G.; Greco, G.; La Magna, A.; Roccaforte, F.; Pécz, B.; Yakimova, R.; Dagher, R.; Michon, A.; Cordier, Y., Graphene integration with nitride semiconductors for high power and high frequency electronics. *Phys. Status Solidi A* **2017,** *214* (4).

26. Barrios, E. L.; Ursúa, A.; Marroyo, L.; Sanchis, P., Analytical design methodology for litz-wired high-frequency power transformers. *IEEE Trans. Ind. Electron.* **2015,** *62* (4), 2103-2113.

27. El-Refaie, A. M.; Alexander, J. P.; Galioto, S.; Reddy, P. B.; Huh, K.-K.; de Bock, P.; Shen, X., Advanced high-power-density interior permanent magnet motor for traction applications. *IEEE Trans. Ind. Appl.* **2014,** *50* (5), 3235-3248.

28. Lu, D.; Wong, C., *Materials for advanced packaging, second edition*. 2nd ed.; Springer: Switzerland, 2017; Vol. 181.

29. Jin, F.-L.; Li, X.; Park, S.-J., Synthesis and application of epoxy resins: A review. *J. Ind. Eng. Chem.* **2015,** *29*, 1-11.

30. Mailhot, B.; Morlat‐Thérias, S.; Ouahioune, M.; Gardette, J. L., Study of the degradation of an epoxy/amine resin, 1. *Macromol. Chem. Phys.* **2005,** *206* (5), 575-584.

31. Pei, Y.-m.; Wang, K.; Zhan, M.-s.; Xu, W.; Ding, X.-j., Thermal-oxidative aging of DGEBA/EPN/LMPA epoxy system: Chemical structure and thermal–mechanical properties. *Polym. Degrad. Stab.* **2011,** *96* (7), 1179-1186.

32. Yang, Y.; Xian, G.; Li, H.; Sui, L., Thermal aging of an anhydride-cured epoxy resin. *Polym. Degrad. Stab.* **2015,** *118*, 111-119.

33. Gigliotti, M.; Minervino, M.; Lafarie-Frenot, M.; Grandidier, J., Effect of thermo-oxidation on the local mechanical behaviour of epoxy polymer materials for high temperature applications. *Mech. Mater.* **2016,** *101*, 118-135.

34. Zhao, Q.; Wang, X.-y.; Hu, Y.-h., The application of highly soluble amine-terminated aromatic polyimides with pendent tert-butyl groups as a tougher for epoxy resin. *Chin. J. Polym. Sci.* **2015,** *33* (10), 1359-1372.

35. Lee, S.; Yoo, T.; Han, Y.; Kim, H.; Han, H., Polyimide–Epoxy Composites with Superior Bendable Properties for Application in Flexible Electronics. *J. Electron. Mater.* **2017,** *46* (8), 4740-4749.

36. Konnola, R.; Parameswaranpillai, J.; Joseph, K., Mechanical, thermal, and viscoelastic response of novel in situ CTBN/POSS/epoxy hybrid composite system. *Polym. Compos.* **2016,** *37* (7), 2109-2120.

37. Thitsartarn, W.; Fan, X.; Sun, Y.; Yeo, J. C. C.; Yuan, D.; He, C., Simultaneous enhancement of strength and toughness of epoxy using POSS-Rubber core–shell nanoparticles. *Compos. Sci. Technol.* **2015,** *118*, 63-71.

38. Song, S. H.; Park, K. H.; Kim, B. H.; Choi, Y. W.; Jun, G. H.; Lee, D. J.; Kong, B. S.; Paik, K. W.; Jeon, S., Enhanced Thermal Conductivity of Epoxy‐Graphene Composites by Using Non‐Oxidized Graphene Flakes with Non‐Covalent Functionalization. *Adv. Mater.* **2013,** *25* (5), 732-737.

39. Martin-Gallego, M.; Verdejo, R.; Lopez-Manchado, M.; Sangermano, M., Epoxy-graphene UV-cured nanocomposites. *Polymer* **2011,** *52* (21), 4664-4669.

40. Ma, Q.; Luo, J.; Chen, Y.; Wei, W.; Liu, R.; Liu, X., Reactive copolymer functionalized graphene sheet for enhanced mechanical and thermal properties of epoxy composites. *J. Polym. Sci. A* **2015,** *53* (23), 2776-2785.

41. Cha, J.; Jin, S.; Shim, J. H.; Park, C. S.; Ryu, H. J.; Hong, S. H., Functionalization of carbon nanotubes for fabrication of CNT/epoxy nanocomposites. *Mater. Des.* **2016,** *95*, 1-8.

42. Ma, C.; Liu, H.-Y.; Du, X.; Mach, L.; Xu, F.; Mai, Y.-W., Fracture resistance, thermal and electrical properties of epoxy composites containing aligned carbon nanotubes by low magnetic field. *Compos. Sci. Technol.* **2015,** *114*, 126-135.

43. Garimella, S. V.; Fleischer, A. S.; Murthy, J. Y.; Keshavarzi, A.; Prasher, R.; Patel, C.; Bhavnani, S. H.; Venkatasubramanian, R.; Mahajan, R.; Joshi, Y., Thermal challenges in next-generation electronic systems. *IEEE Trans. Compon. Packag. Technol.* **2008,** *31* (4), 801-815.

44. Johnson, R. W.; Evans, J. L.; Jacobsen, P.; Thompson, J. R.; Christopher, M., The changing automotive environment: high-temperature electronics. *IEEE Trans. Electron. Packag. Manuf.* **2004,** *27* (3), 164-176.

45. Yang, D.-G.; Wan, F.; Shou, Z.; van Driel, W. D.; Scholten, H.; Goumans, L.; Faria, R., Effect of high temperature aging on reliability of automotive electronics. *Microelectron. Reliab.* **2011,** *51* (9), 1938-1942.

46. Braun, T.; Becker, K.-F.; Koch, M.; Bader, V.; Aschenbrenner, R.; Reichl, H., Reliability potential of epoxy based encapsulants for automotive applications. *Microelectron. Reliab.* **2005,** *45* (9-11), 1672-1675.

47. Hamerton, I., *Chemistry and technology of cyanate ester resins*. Blackie Academic & Professional: Glasgow, 1994.

48. Ramirez, M. L.; Walters, R.; Lyon, R. E.; Savitski, E. P., Thermal decomposition of cyanate ester resins. *Polym. Degrad. Stab.* **2002,** *78* (1), 73-82.

49. Toldy, A.; Szlancsik, Á.; Szolnoki, B., Reactive flame retardancy of cyanate ester/epoxy resin blends and their carbon fibre reinforced composites. *Polym. Degrad. Stab.* **2016,** *128*, 29-38.

50. Lin, C. H., Synthesis of novel phosphorus-containing cyanate esters and their curing reaction with epoxy resin. *Polymer* **2004,** *45* (23), 7911-7926.

51. Liang, G.; Zhang, M., Enhancement of processability of cyanate ester resin via copolymerization with epoxy resin. *J. Appl. Polym. Sci.* **2002,** *85* (11), 2377-2381.

52. Ren, F.; Zhu, G.; Ren, P.; Wang, Y.; Cui, X., In situ polymerization of graphene oxide and cyanate ester–epoxy with enhanced mechanical and thermal properties. *Appl. Surf. Sci.* **2014,** *316*, 549-557.

53. Martin, M.; Ormaetxea, M.; Harismendy, I.; Remiro, P.; Mondragon, I., Cure chemo-rheology of mixtures based on epoxy resins and ester cyanates. *Eur. Polym. J.* **1999,** *35* (1), 57-68.

54. Zhou, C.; Gu, A.; Liang, G.; Yuan, L., Novel toughened cyanate ester resin with good dielectric properties and thermal stability by copolymerizing with hyperbranched polysiloxane and epoxy resin. *Polymers for Advanced Technologies* **2011,** *22* (5), 710-717.

55. Ren, P.; Liang, G.; Zhang, Z., Epoxy‐modified cyanate ester resin and its high‐modulus carbon‐fiber composites. *Polym. Compos.* **2006,** *27* (4), 402-409.

56. Lin, C. H.; Huang, C. M.; Wong, T. I.; Chang, H. C.; Juang, T. Y.; Su, W. C., High‐Tg and low‐dielectric epoxy thermosets based on a propargyl ether‐containing phosphinated benzoxazine. *J. Polym. Sci. A* **2014,** *52* (9), 1359-1367.

57. Kollia, E.; Loutas, T.; Fiamegkou, E.; Vavouliotis, A.; Kostopoulos, V., Degradation behavior of glass fiber reinforced cyanate ester composites under hydrothermal ageing. *Polym. Degrad. Stab.* **2015,** *121*, 200-207.

58. Guo, B.; Jia, D.; Fu, W.; Qiu, Q., Hygrothermal stability of dicyanate-novolac epoxy resin blends. *Polym. Degrad. Stab.* **2003,** *79* (3), 521-528.

59. Dang, D. N.; Cohendoz, S.; Mallarino, S.; Feaugas, X.; Touzain, S., Effects of curing program on mechanical behavior and water absorption of DGEBA/TETa epoxy network. *J. Appl. Polym. Sci.* **2013,** *129* (5), 2451-2463.

60. Liu, Z.; Huo, J.; Yu, Y., Water absorption behavior and thermal-mechanical properties of epoxy resins cured with cardanol-based novolac resins and their esterified ramifications. *Materials Today Communications* **2017,** *10*, 80-94.

61. Karad, S. K.; Attwood, D.; Jones, F. R., Moisture absorption by cyanate ester modified epoxy resin matrices. Part III. Effect of blend composition. *Compos. Part A Appl. Sci. Manuf.* **2002,** *33* (12), 1665-1675.

62. Pérez-Pacheco, E.; Cauich-Cupul, J.; Valadez-González, A.; Herrera-Franco, P., Effect of moisture absorption on the mechanical behavior of carbon fiber/epoxy matrix composites. *J. Mater. Sci.* **2013,** *48* (5), 1873-1882.

63. Wong, K.; Low, K.; Israr, H.; Tamin, M., Thickness-dependent non-Fickian moisture absorption in epoxy molding compounds. *Microelectron. Reliab.* **2016,** *65*, 160-166.

64. Fan, X.; Lee, S.; Han, Q., Experimental investigations and model study of moisture behaviors in polymeric materials. *Microelectron. Reliab.* **2009,** *49* (8), 861-871.

65. Khazaka, R.; Mendizabal, L.; Henry, D.; Hanna, R., Survey of high-temperature reliability of power electronics packaging components. *IEEE Trans. Power Electron.* **2015,** *30* (5), 2456-2464.

66. Locatelli, M.-L.; Khazaka, R.; Diaham, S.; Pham, C.-D.; Bechara, M.; Dinculescu, S.; Bidan, P., Evaluation of encapsulation materials for High-Temperature power device packaging. *IEEE Trans. Power Electron.* **2014,** *29* (5), 2281-2288.

67. Wang, X.; Hu, Y.; Song, L.; Xing, W.; Lu, H., Thermal degradation behaviors of epoxy resin/POSS hybrids and phosphorus–silicon synergism of flame retardancy. *J. Polym. Sci. B Polym. Phys.* **2010,** *48* (6), 693-705.

68. Li, Q.; Chen, L.; Gadinski, M. R.; Zhang, S.; Zhang, G.; Li, H. U.; Iagodkine, E.; Haque, A.; Chen, L.-Q.; Jackson, T. N., Flexible high-temperature dielectric materials from polymer nanocomposites. *Nature* **2015,** *523* (7562), 576.

69. Tuan, C.-C.; Wu, F.; Moon, K.-S.; Wong, C.-P. In *Epoxy/cyanate ester copolymer material for molding compounds in high-temperature operations*, Electronic Components and Technology Conference (ECTC), 2017 IEEE 67th, IEEE: 2017; pp 1328-1333.

70. Wu, F.; Tuan, C.-C.; Song, B.; Moon, K.-S.; Wong, C.-P., Controlled Synthesis and Evaluation of Cyanate Ester/Epoxy Copolymer System for High Temperature Molding Compounds. *J. Polym. Sci. A Polym. Chem.* **2018**.

71. Lin, C. H.; Chou, Y. C.; Shiao, W. F.; Wang, M. W., High temperature, flame-retardant, and transparent epoxy thermosets prepared from an acetovanillone-based hydroxyl poly (ether sulfone) and commercial epoxy resins. *Polymer* **2016,** *97*, 300-308.

72. Braun, U.; Knoll, U.; Schartel, B.; Hoffmann, T.; Pospiech, D.; Artner, J.; Ciesielski, M.; Döring, M.; Perez‐Graterol, R.; Sandler, J. K., Novel Phosphorus‐Containing Poly (ether sulfone) s and Their Blends with an Epoxy Resin: Thermal Decomposition and Fire Retardancy. *Macromol. Chem. Phys.* **2006,** *207* (16), 1501-1514.

73. Wu, C.-S.; Liu, Y.-L.; Hsu, K.-Y., Maleimide-epoxy resins: preparation, thermal properties, and flame retardance. *Polymer* **2003,** *44* (3), 565-573.

74. Huang, Y. J.; Ye, Y. S.; Yen, Y. C.; Tsai, L. D.; Hwang, B. J.; Chang, F. C., Synthesis and characterization of new sulfonated polytriazole proton exchange membrane by click reaction for direct methanol fuel cells (DMFCs). *Int. J. Hydrog. Energy* **2011,** *36* (23), 15333-15343.

75. Park, S.; Kim, K.; Kim, D. M.; Kwon, W.; Choi, J.; Ree, M., High temperature polyimide containing anthracene moiety and its structure, interface, and nonvolatile memory behavior. *ACS Appl. Mater. Interfaces* **2011,** *3* (3), 765-773.

76. Jiang, W.; Liu, Z.; Kong, Q.; Yao, J.; Zhang, C.; Han, P.; Cui, G., A high temperature operating nanofibrous polyimide separator in Li-ion battery. *Solid State Ionics* **2013,** *232*, 44-48.

77. Yoonessi, M.; Shi, Y.; Scheiman, D. A.; Lebron-Colon, M.; Tigelaar, D. M.; Weiss, R.; Meador, M. A., Graphene polyimide nanocomposites; thermal, mechanical, and high-temperature shape memory effects. *ACS nano* **2012,** *6* (9), 7644-7655.

78. Zelmat, S.; Locatelli, M.-L.; Lebey, T.; Diaham, S., Investigations on high temperature polyimide potentialities for silicon carbide power device passivation. *Microelectron. Eng.* **2006,** *83* (1), 51-54.

79. Ni, H.-j.; Liu, J.-g.; Wang, Z.-h.; Yang, S.-y., A review on colorless and optically transparent polyimide films: Chemistry, process and engineering applications. *J. Ind. Eng. Chem.* **2015,** *28*, 16-27.

80. Lee, C. H.; Wang, Y. Z., Synthesis and characterization of epoxy‐based semi‐interpenetrating polymer networks sulfonated polyimides proton‐exchange membranes for direct methanol fuel cell applications. *J. Polym. Sci. A Polym. Chem.* **2008,** *46* (6), 2262-2276.

81. Jin, F. L.; Park, S. J., Thermal properties and toughness performance of hyperbranched‐polyimide‐modified epoxy resins. *J. Polym. Sci. B Polym. Phys.* **2006,** *44* (23), 3348-3356.

82. Bakar, M.; Okulska-Bożek, M.; Zygmunt, M., Effect of poly (amic acid) and polyimide on the adhesive strength and fracture toughness of epoxy resin. *Mater. Sci.* **2011,** *47* (3), 355-362.

83. Ohno, D.; Zenyoji, K.; Kurihara, Y.; Ueda, K.; Habuka, H., Formation of Hybrid Ring Structure of Cyanurate/Isocyanurate in the Reaction be-tween 2, 4, 6-Tris (4-Phenyl-Phenoxy)-1, 3, 5-Triazine and Phenyl Glycidyl Ether. *Int. J. Org. Chem.* **2016,** *6* (2).

84. Fang, T.; Shimp, D. A., Polycyanate esters: science and applications. *Prog. Polym. Sci.* **1995,** *20* (1), 61-118.

85. Wang, X.; Jin, J.; Song, M., Cyanate ester resin/graphene nanocomposite: curing dynamics and network formation. *Eur. Polym. J.* **2012,** *48* (6), 1034-1041.

86. So, H. H.; Cho, J. W.; Sahoo, N. G., Effect of carbon nanotubes on mechanical and electrical properties of polyimide/carbon nanotubes nanocomposites. *Eur. Polym. J.* **2007,** *43* (9), 3750-3756.

87. Xie, S.-H.; Zhu, B.-K.; Wei, X.-Z.; Xu, Z.-K.; Xu, Y.-Y., Polyimide/BaTiO3 composites with controllable dielectric properties. *Compos. Part A Appl. Sci. Manuf.* **2005,** *36* (8), 1152-1157.

88. Uemura, T.; Kaseda, T.; Sasaki, Y.; Inukai, M.; Toriyama, T.; Takahara, A.; Jinnai, H.; Kitagawa, S., Mixing of immiscible polymers using nanoporous coordination templates. *Nat. Commun.* **2015,** *6*, 7473.

89. Kim, B. S.; Chiba, T.; Inoue, T., Morphology development via reaction-induced phase separation in epoxy/poly (ether sulfone) blends: morphology control using poly (ether sulfone) with functional end-groups. *Polymer* **1995,** *36* (1), 43-47.

90. Mustata, F.; Bicu, I., Rheological and thermal behaviour of DGEBA/EA and DGEHQ/EA epoxy systems crosslinked with TETA. *Polym. Test.* **2001,** *20* (5), 533-538.

91. Ratna, D.; Simon, G., Thermomechanical properties and morphology of blends of a hydroxy-functionalized hyperbranched polymer and epoxy resin. *Polymer* **2001,** *42* (21), 8833-8839.

92. Mimura, K.; Ito, H.; Fujioka, H., Improvement of thermal and mechanical properties by control of morphologies in PES-modified epoxy resins. *Polymer* **2000,** *41* (12), 4451-4459.

93. Bockenheimer, C.; Fata, D.; Possart, W., New aspects of aging in epoxy networks. I. Thermal aging. *J. Appl. Polym. Sci.* **2004,** *91* (1), 361-368.

94. Chen, J.-S.; Ober, C. K.; Poliks, M. D.; Zhang, Y.; Wiesner, U.; Cohen, C., Controlled degradation of epoxy networks: analysis of crosslink density and glass transition temperature changes in thermally reworkable thermosets. *Polymer* **2004,** *45* (6), 1939-1950.

95. Jin, H.; Yang, B.; Jin, F.-L.; Park, S.-J., Fracture toughness and surface morphology of polysulfone-modified epoxy resin. *J. Ind. Eng. Chem.* **2015,** *25*, 9-11.

96. Gu, X.; Zhang, Z.; Yuan, L.; Liang, G.; Gu, A., Developing high performance cyanate ester resin with significantly reduced postcuring temperature while improved toughness, rigidity, thermal and dielectric properties based on manganese-Schiff base hybridized graphene oxide. *Chem. Eng. J.* **2016,** *298*, 214-224.

97. Bortz, D. R.; Heras, E. G.; Martin-Gullon, I., Impressive fatigue life and fracture toughness improvements in graphene oxide/epoxy composites. *Macromolecules* **2011,** *45* (1), 238-245.

98. Wong, D. W.; Lin, L.; McGrail, P. T.; Peijs, T.; Hogg, P. J., Improved fracture toughness of carbon fibre/epoxy composite laminates using dissolvable thermoplastic fibres. *Compos. Part A Appl. Sci. Manuf.* **2010,** *41* (6), 759-767.

99. Zhang, D.; Jia, D., Toughness and strength improvement of diglycidyl ether of bisphenol‐A by low viscosity liquid hyperbranched epoxy resin. *J. Appl. Polym. Sci.* **2006,** *101* (4), 2504-2511.

100. Fei, X.; Zhao, F.; Wei, W.; Luo, J.; Chen, M.; Liu, X., Tannic acid as a bio-based modifier of epoxy/anhydride thermosets. *Polymers* **2016,** *8* (9), 314.

101. Liu, T.; Nie, Y.; Chen, R.; Zhang, L.; Meng, Y.; Li, X., Hyperbranched polyether as an all-purpose epoxy modifier: controlled synthesis and toughening mechanisms. *J. Mater. Chem. A* **2015,** *3* (3), 1188-1198.

102. Decelle, J.; Huet, N.; Bellenger, V., Oxidation induced shrinkage for thermally aged epoxy networks. *Polym. Degrad. Stab.* **2003,** *81* (2), 239-248.

103. Delor-Jestin, F.; Drouin, D.; Cheval, P.-Y.; Lacoste, J., Thermal and photochemical ageing of epoxy resin–Influence of curing agents. *Polym. Degrad. Stab.* **2006,** *91* (6), 1247-1255.

104. Paplham, W.; Brown, R.; Salin, I.; Seferis, J., Absorption of water in polyimide resins and composites. *J. Appl. Polym. Sci.* **1995,** *57* (2), 133-137.

105. Merdas, I.; Thominette, F.; Verdu, J., Humid aging of polyetherimide. I. Water sorption characteristics. *J. Appl. Polym. Sci.* **2000,** *77* (7), 1439-1444.

106. Huang, X.; Jiang, P.; Tanaka, T., A review of dielectric polymer composites with high thermal conductivity. *IEEE Electrical Insulation Magazine* **2011,** *27* (4).

107. Kozako, M.; Okazaki, Y.; Hikita, M.; Tanaka, T. In *Preparation and evaluation of epoxy composite insulating materials toward high thermal conductivity*, Solid Dielectrics (ICSD), 2010 10th IEEE international conference on, IEEE: 2010; pp 1-4.

108. Lee, G.-W.; Park, M.; Kim, J.; Lee, J. I.; Yoon, H. G., Enhanced thermal conductivity of polymer composites filled with hybrid filler. *Composites Part A: Applied science and manufacturing* **2006,** *37* (5), 727-734.

109. Liang, Q.; Moon, K.-S.; Jiang, H.; Wong, C. P., Thermal conductivity enhancement of epoxy composites by interfacial covalent bonding for underfill and thermal interfacial materials in Cu/Low-K application. *IEEE Transactions on Components, Packaging and Manufacturing Technology* **2012,** *2* (10), 1571-1579.

110. Lundqvist, D., On the crystal structure of silicon carbide and its content of impurities. *Acta Chemica Scandinavica* **1948,** *2* (1), 177.

111. McIntyre, G.; Mádési, L.; Guthrie, M.; Tulk, C.; Xu, J.; Parise, J., One picture says it all—high-pressure cells for neutron Laue diffraction on VIVALDI. *Journal of Physics: Condensed Matter* **2005,** *17* (40), S3017.

112. Martínez, J.; Palomares-Sánchez, S.; Ortega-Zarzosa, G.; Ruiz, F.; Chumakov, Y., Rietveld refinement of amorphous SiO2 prepared via sol–gel method. *Materials letters* **2006,** *60* (29-30), 3526-3529.

113. A. Jadhav, S.; Bongiovanni, R.; L. Marchisio, D.; Fontana, D.; Egger, C., Surface modification of iron oxide (Fe2O3) pigment particles with amino-functional polysiloxane for improved dispersion stability and hydrophobicity. *Pigment & Resin Technology* **2014,** *43* (4), 219-227.

114. Zhou, T.; Wang, X.; Liu, X.; Xiong, D., Improved thermal conductivity of epoxy composites using a hybrid multi-walled carbon nanotube/micro-SiC filler. *Carbon* **2010,** *48* (4), 1171-1176.

115. Chandrasekaran, S.; Sato, N.; Tölle, F.; Mülhaupt, R.; Fiedler, B.; Schulte, K., Fracture toughness and failure mechanism of graphene based epoxy composites. *Composites Science and Technology* **2014,** *97*, 90-99.

116. Baick, I. H.; Lee, M. S.; Lee, M.; Kim, B.; Ha, S. S.; Jeong, S. W.; Kim, M.; Pae, S. In *Effect of EMC properties on the chip to package interaction (CPI) reliability of flip chip package*, Integrated Reliability Workshop (IIRW), 2017 IEEE International, IEEE: 2017; pp 1-6.

117. Lee, K.; Kim, M. S.; Kim, J.; Kim, S.; Lee, D.; Jung, K. In *Improvement of package warpage through substrate and EMC optimization*, Semiconductor Technology International Conference (CSTIC), 2018 China, IEEE: 2018; pp 1-4.

118. Zhu, S.; Ding, S.; Wang, R., Low-temperature fabrication of porous SiC ceramics by preceramic polymer reaction bonding. *Materials Letters* **2005,** *59* (5), 595-597.

119. Matus, Y. B.; De Jonghe, L. C.; Jacobson, C. P.; Visco, S. J., Metal-supported solid oxide fuel cell membranes for rapid thermal cycling. *Solid State Ionics* **2005,** *176* (5-6), 443-449.

120. Ley, K.; Krumpelt, M.; Kumar, R.; Meiser, J.; Bloom, I., Glass-ceramic sealants for solid oxide fuel cells: Part I. Physical properties. *Journal of Materials Research* **1996,** *11* (6), 1489-1493.